Departament d'Enginyeria Mecànica

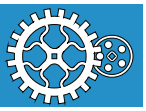

UNIVERSITAT POLITÈCNICA DE CATALUNYA

Passive acoustic method for aircraft localization

by

Sara-Regina Martín Román

directed by

Jordi Romeu Garbí

Meritxell Genescà i Francitorra

A thesis submitted in partial fulfillment for the
degree of Doctor of Philosophy of Mechanical Engineering

in the

Escola Tècnica Superior d'Enginyeries Industrial i Aeronàutica de Terrassa

Department of Mechanical Engineering

May 2013

If I have been able to see further, it was only because I stood on the shoulders of giants.

Isaac Newton

Abstract

Escola Tècnica Superior d'Enginyeries Industrial i Aeronàutica de Terrassa
Department of Mechanical Engineering

Doctor of Philosophy in Mechanical Engineering

by Sara-Regina Martín Román

The present thesis investigates a passive acoustic method to locate maneuvering aircraft. The method is based on the acoustical Doppler effect, as a particular effect of the signals received by a mesh of spatially distributed microphones. A one-dimensional version of the ambiguity function allows for the calculation of the frequency stretch factor that occurs between the sound signals received by a pair of microphones. The mathematical expression for this frequency stretch is a function of the aircraft position and velocity, both of them being estimated by a genetic algorithm. The method requires only a minimum of seven microphones and the prior knowledge of the aircraft position and velocity at a given time. The advantages of the method are that it is suitable for all kind of aircraft, not only propeller-driven, and is not restricted to low heights above the ground. Its applicability could be, for instance, to supplement aircraft noise monitoring systems or to supervise small airports activities. This doctoral research includes the theoretical background of the method as well as the detailed description of its implementation. To assess the performance of the method, results from computer simulations are discussed. First of all, noise propagation is considered in a lossless medium, thus only geometrical spreading influences the sound emitted by the source traveling to the receivers. The accuracy of each step of the method has been evaluated and the results obtained reveal acceptable performance. Due to the large distances between microphones and the aircraft in flight, the atmospheric attenuation plays a major roll. Therefore, computer simulations have also been carried out under the assumption of an homogeneous but non lossless medium to evaluate the influence of the atmospheric absorption on the aircraft location. Under these conditions, the performance of the method with respect to the microphone distribution is discussed. Moreover, the location method has also been tested for a possible inaccuracy on the microphones synchronization. Finally, an outdoor experimental validation of the acoustic method has been carried out with a radio control airplane. The description of the experimental test is detailed in the present work as well as the results obtained.

Acknowledgements

Vull agraïr en primer lloc el suport incondicional i la confiança dispensada pels dos directors d'aquesta tesis, Meritxell Genescà i Jordi Romeu. La seva dedicació i el seu consell han estat imprescindibles al llarg d'aquests quatre anys de recerca.

Esmentar també amb agraïment a tots i cada un dels meus companys del laboratori: Teresa, Santi, Andreu, i en especial els qui han compartit el despatx 1.02 amb mi durant tot el trajecte doctoral: Arnau, Julen i Robert.

Por otro lado, deseo también manifestar que esta tesis no hubiera sido posible sin el apoyo y el cariño de mi entorno familiar, especialmente de mis padres, Josefina y Francisco, de mi hermana Nadia y de Pablo. A ellos dedico este trabajo, resultado de un esfuerzo personal que tanto sacrificio ha significado para todos ellos.

A María Eugenia e Ciriaco, que tan ben comprenderon o importante que era para min sacar adiante este proxecto

I finalment recordar a tots els qui no esmento en aquest escrit, que saben, tant ells com jo que han estat essencials per dur a bon port aquest treball. A tots, moltes gràcies.

Contents

To my Mum and my Dad
To Nadia and Pablo

Chapter 1

Introduction

The main purpose of the present thesis is to design, implement and validate a passive acoustic method for aircraft localization in the vicinity of an airport. This method is developed for environmental purposes as a complement to a noise monitoring system (NMS). The goal is to suppress the current dependence of noise monitoring systems on RADAR data. This thesis is part of a bigger project aiming to obtain the real aircraft sound power levels to monitor the acoustic impact of an airport in its surroundings. This integrated noise monitoring system would have the same structure as the current ones, a mesh of noise measuring terminals (NMT) distributed in the acoustic area of influence of the airport, and would provide both the position and sound power of the aircraft. Using these data as input to a propagation model, the real aircraft acoustic footprint could be reconstructed. The present thesis focuses on the first challenge of the noise monitoring project concerning the passive acoustic localization of the aircraft.

Currently, noise monitoring systems are used to control and evaluate the noise emitted by an aircraft in the surroundings of an airport. Commercial aircraft noise monitoring systems are integrated by a mesh of noise monitoring terminals measuring the environmental noise. These data are complemented with external data from the traffic control radar, with meteorological data, and sometimes even with data from systems collecting citizens complains related to aircraft noise.

One of the main problems of the NMS is the influence of background noise on the noise recordings at the NMT. The ISO20906 *Acoustic unattended monitoring of aircraft sound in the vicinity of airports* [1], defines the procedure to distinguish noise events associated to aircraft flyover from other noise events. First, a sound level threshold has to be set

and used as a trigger on the noise recording to select potential aircraft noise events. In that way, noise events too low to be generated by aircraft fly-over are directly discarded.

Then, the next step is to assess the duration of the noise event exceeding the established threshold in conjunction with the noise level evolution. The noise event has to last for a minimum amount of time to be attributed to an aircraft operation. This condition allows discarding, for instance, loud and very short events that surely are not caused by any aircraft operation.

Afterwards, the selected noise events are correlated with flight tracking data to ensure that the source of the noise event can be an aircraft. RADAR data are often provided with some delay for security purposes disabling the option of real-time aircraft noise discrimination, and moreover, in small airports where light aircrafts operate these data are often not available at all.

The present work focuses on solving this dependency problem and introduces a new passive acoustic method providing the aircraft flight trajectory. This system could complement a NMS and make it totally independent from non-acoustical data. The method could successfully provide a tool to concerned entities, external to the airport, in order to ensure the accomplishment of flight path procedures, as well as a low budget instrument for small airports with no radar system, enabling their managers to control physical location of airplanes. It may be also useful for military purposes such as battlefield surveillance, border control, disarmament verification or peacekeeping agreements.

The thesis is organized as follows. Chapter 2 presents the state of the art of the different acoustic techniques suggested in the literature for aircraft localization purposes. Chapter 3 exposes the theoretical background and the implementation description of the new acoustic localization method. Chapter 4 analyzes the results obtained from computer simulation. And finally, chapter 5 describes the experimental validation of the method carried out and discusses the results obtained.

Chapter 2

Review of acoustic techniques for aircraft localization

RADAR systems are the most commonly used systems for aircraft tracking [2, 3]. Their implementation requires complex and expensive devices, especially for small airports and may fail when the tracking target is in non-line-of-sight or when electromagnetic radiation interferes with system operations [4]. As an alternative, different acoustical techniques aimed at locating an aircraft in flight have been presented in the literature.

Some of these acoustic methods have been developed depending on the type of target, some methods are suitable for all kind of aircraft, and other methods are just suitable for those with tonal noise components (propeller driven aircraft or helicopter). Most of the general methods that can be used regardless of the aircraft type rely on the time delay estimation between the elements of an array of sensors to locate the source. When limiting the location to such a low altitude that the wave fronts can be considered spherical, a planar microphone array can provide both the bearing and range of the source. Ref.[5] describes a method to locate low altitude moving sources using a planar microphone array of 5 sensors. The five identical omnidirectional microphones are distributed in the (xy)-plane, one of them as the origin of the Cartesian coordinate system and the others are diametrically opposed in both axes (Ox) and (Oy) as showed in fig.2.1. With this configuration, the target range, azimuth angle and elevation angle are derived from the geometric relations between the target and the acoustic array and are expressed as a function of the signal delay between the sensors $1-4$ and the origin sensor 0.

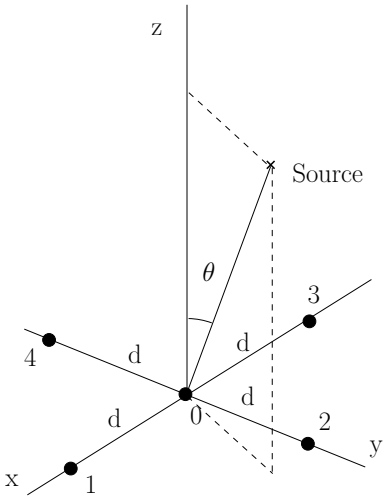

FIGURE 2.1: Array used in ref.[5]

Ref.[6] suggests a method to estimate the position of the sound source as a function of time using different microphone array geometries. The method estimates the flight parameters (i.e., the source speed, the time at which the source is at the closest point of approach (cpa) of one of the sensors, the source distance to that sensor, the source altitude and the source azimuth angle at cpa) in the case of an aircraft flying at a fixed altitude and velocity. Both in [5] and [6] the distance between the microphones included in the array, is small enough that the Doppler effect is assumed to affect the signals of all the receivers in the same way. In the case of having a large aperture array, the Doppler effect causes the time scale to be different for each receiver and therefore the conventional cross-correlation techniques to fail at estimating the time delay. In [7] and [8] the wide band correlation function is used to compensate for the differential Doppler stretch, in order to obtain an acceptable estimation of the time delay.

Under the spherical wavefront assumption, linear microphone arrays have been used as well in the case that some information on the source path is available. Ref.[9] describes a method to determine the range and bearing of a generic source by using a linear microphone array of at least 3 elements. Ref.[10] uses this method to experimentally obtain the instantaneous range of a jet airplane that travels at a constant speed and height from a broadside direction with respect to the array axis and over the array center.

When the airplane is at large distance from the microphone array, the impinging wavefronts are planar, and a planar microphone array can only estimate the bearing of the source (not the range). However, if the plane of movement of the source is known, the

bearing is enough to completely locate the source in the plane of movement, and a planar microphone array is still effective. Ref.[11] describes and tests a method for aircraft tracking in ground operations with a planar array of 105 microphones situated in concentric circles. The extraction of individual frequency bins from the broadband signal emitted by the aircraft allows for a narrow-band approach. From the 105 microphones, only 45 are processed per bin and the process of several bins is combined for wideband detection purposes.

In the case that the airplane flies at a constant height and speed, there have been attempts to estimate the motion parameters (i.e, the velocity, direction of flight, cpa distance, height of the flight, path above ground, and azimuth and elevation angles of the cpa) from a single microphone array. Ref.[12] analyzes the performance of a 4 microphone spherical array (fig.2.2) to obtain the motion parameters of helicopters, jet and propeller-driven aircrafts traveling along a straight line at a constant speed and height. However, if the target is a maneuvering source, triangulation between multiple nodes is required to completely localize the source. Every node estimates the bearing of the source with respect to the node position, which is accurately known. It has to be taken into account the fact that the signal received at the same time by all the nodes was not emitted at the same time, and therefore does not correspond to the same position of the source. Ref.[13] describes a method to track maneuvering aircraft from a net of at least 2 nodes separated hundreds of meters that provide the source bearing. Refs.[14] and [15] are focussed in developing efficient algorithms to track the source in the horizontal plane from the azimuth estimates provided by the nodes. Ref.[16] describes a possible structure of the nodes and a local signal processing algorithm to obtain the azimuth of the source. The nodes are integrated by a 9-microphone planar array lying on the ground, and the bearing is found by computing the wavenumber power spectra for every steering direction and selecting the angles corresponding to the peaks. Ref.[17] uses a two 4-microphone spherical arrays at a distance of 150 m from each other to obtain the bearing of the source and describes how to track the source by triangulation. Ref.[18] uses a similar method to localize gun shots, although it uses a pair of planar arrays of 3 microphones separated several kilometers to localize the source just in the horizontal plane. Refs.[19] and [20] also present a similar method to measure a moving source bearing using an acoustic vector sensor that measures the acoustic pressure and the three components of the velocity instead of a microphone array.

As an alternative to the use of microphone arrays, ref.[21] suggests the use of a single receiver to estimate the flight parameters of an aircraft that flies in a straight line, at

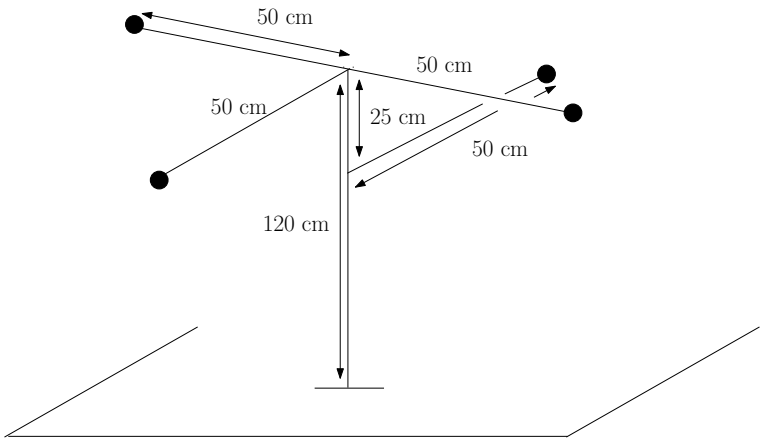

FIGURE 2.2: Array used in ref.[12]

constant speed, and altitude over a hard ground. This method uses the fact that the time-frequency patterns of interference between the direct and the reflected sound change as a function of the source position. The values of the flight parameters are obtained by fitting an interference theoretical model to the time-frequency interference pattern measured by the receiver. The same author in ref.[22] proposes another method to obtain the flight parameters with a single receiver by means of the time delay observed between the direct and the reflected sound. In this case the flight parameters are obtained by adjusting a theoretical model of the temporal evolution of the time delay as a function of the flight parameters, to the time delay evolution measured by the receiver.

In the case of propeller driven aircraft which have a tonal noise spectrum, there are several methods to obtain the flight parameters of an aircraft flying at a constant speed and with a constant velocity. They rely on the Doppler effect on a single receiving point to localize the source. Refs.[8] and [23] use a single receiver located directly below the aircraft flight path to obtain the speed, the cpa distance, and original frequency from the temporal evolution of the instantaneous frequency. In ref.[10] this method is experimentally tested and compared to the method presented in ref.[6]. To also obtain the source height and horizontal distance (closest horizontal distance from the reference receiver to the source), ref.[24] uses a set of distributed receivers and a nonlinear least squares method. Ref.[25] explores the case of having the receiver towed below the sea surface, and an aircraft flying at constant altitude, speed, and direction, and its cpa being directly over the receiver. In this case, the receiver needs to be integrated by an array of hydrophones instead of a single receiver, so it can distinguish between the direct sound, and the sound reflected from the sea bottom. By using the observed Doppler shift and apparent bearing information, the method is able to estimate the aircraft's

horizontal range, speed, direction, and altitude. The speed is obtained from the signal's reflection on the bottom, and the height of the plane is obtained from the direct signal. Ref.[26] uses an acoustic vector sensor to complement the technique used in ref.[23] which provides the speed, the cpa distance, and original frequency. The acoustic vector sensor allows to obtain also the height and the heading of the source from the particle velocity measurement.

The present thesis explores the application of the acoustic source localization method described in ref.[27] to aircraft position estimation. This method uses a mesh of single receivers and relies in the relative Doppler stretch measured between them to locate the source. On comparison with the methods based in the Doppler effect developed previously [8, 23–26], the method described here is suitable for all kind of aircraft, not just propeller-driven. Doppler effect is here considered to stretch the frequency spectrum of the emitted sound source and not to shift it (which is equivalent only in case of single-frequency emission). This means that, because jet noise is broadband, the Doppler effect cannot be considered to shift the frequency axes of the spectrum (as done when the source has a main tonal component like propeller aircraft) but to stretch it.

The present method is not restricted to low altitude targets as the methods that assume spherical sound waves [5, 6, 9, 10], and does not require that the aircraft flies at constant speed and altitude [12, 21, 22] or the plane of movement to be known [11]. The technique described in chapter 3 is different from the methods that locate the aircraft by triangulation of the bearings provided by a set of nodes [13–15] in that the nodes are here integrated by a single microphone. Some of the triangulation methods obtain the source bearing from a microphone array [16–18], and some others from an acoustic vector sensor that measures the sound intensity [19, 20] being, the latter, sensitive to the background noise. The present method is similar to that presented in [8] and [7] in that it uses an array of microphones distributed along a vast area and therefore the differential Doppler stretch has to be taken into account. As in [8] and [7] the wide band ambiguity function is used, but in the present case the location of the aircraft is estimated by using the differential Doppler stretch rather than the time delay between the receiver's signals.

Chapter 3

Description of the new acoustic localization method

3.1 Theoretical background

The passive acoustic method for aircraft localization presented in this thesis uses a mesh of acoustic sensors randomly distributed in the acoustic area of influence in the vicinity of an airport. The aircraft position is derived from the received signals as detailed in the next sections organized as follows. Section 3.1.1 explains the synchronization process of the received signals required to compensate for the Retardation effect influencing all signals registered at different spatial locations. The need of the prior knowledge of an initial aircraft position is highlighted. Section 3.1.2 derives the relation between the Doppler stretch between two different frequency spectra (the relative Doppler stretch) and the position and velocity of the aircraft. In section 3.1.3, the technique used for the computation of the relative Doppler frequency stretch between the broadband signals received at two different locations is explained. Finally, section 3.1.4 summarizes the localization process successively applied to estimate the aircraft flight trajectory.

3.1.1 Retardation effect and signal synchronization

The sound emitted at some time t is received by different acoustic sensors at different time instants, this phenomenon is known as the Retardation effect. Therefore, the signals received at some time t' by different acoustic sensors do not correspond to the same emitted signal.

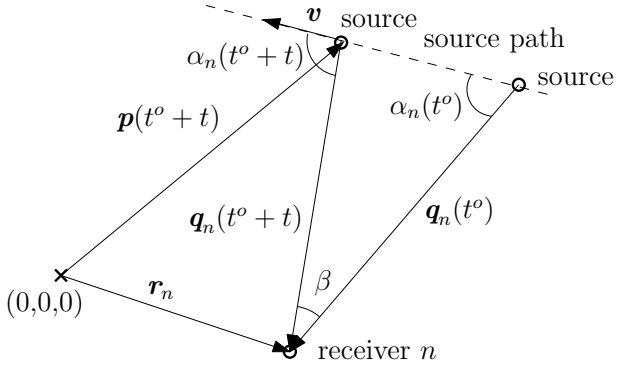

FIGURE 3.1: Geometric relations for pathlength vectors $\boldsymbol{q}_n(t^o)$ at time t^o and $\boldsymbol{q}_n(t^o+t)$ at a later time.

Let c be the speed of the aircraft sound propagated in the air (this thesis assumes an isospeed medium), t^o the initial instant and $\boldsymbol{q}_n(t^o+t)$ the vector from the aircraft to the position of receiver n at some time t^o+t as shown in fig.3.1. The signal emitted t seconds after t^o reaches the receiver n at t'_n+t^o where

$$t'_n = t + \frac{|\boldsymbol{q}_n(t^o+t)|}{c}. \tag{3.1}$$

Therefore, the relation between the received signal y_n and the emitted signal s_e is given by:

$$y_n(t^o+t'_n) = \rho_n \cdot s_e(t^o+t). \tag{3.2}$$

where ρ_n is an amplitude scale factor explained in detail in sections 4.1.1.2 and 4.2.1.2.

The aircraft velocity $\boldsymbol{v}$ and acceleration $\boldsymbol{a}$ can be expressed as follows taking as a moving reference the pathlength vector $\boldsymbol{q}_n(t^o+t)$ provided that no rotation around $\boldsymbol{q}_n(t^o+t)$ is allowed:

$$\boldsymbol{v} = \dot{\boldsymbol{q}}_n(t^o+t) + \dot{\boldsymbol{\beta}} \times (-\boldsymbol{q}_n(t^o+t)) \tag{3.3}$$

$$\boldsymbol{a} = \ddot{\boldsymbol{q}}_n(t^o+t) - \dot{\beta}^2 \cdot (-\boldsymbol{q}_n(t^o+t)) + \ddot{\boldsymbol{\beta}} \times (-\boldsymbol{q}_n(t^o+t)) + 2\dot{\boldsymbol{\beta}} \times \boldsymbol{v} \tag{3.4}$$

Assuming that $|\boldsymbol{v}| \cdot t << |\boldsymbol{q}_n(t^o)|$ which means that the distance traveled by the aircraft during a small portion of time lasting t s is much smaller than the distance between the aircraft and receiver n, the angular velocity of the vector $\boldsymbol{q}_n$, $\dot{\beta}$, is negligible, and thus β is so small that can be also neglected. If β is negligible and t small enough that the aircraft velocity $\boldsymbol{v}$ can be considered constant, α_n can also be considered constant. Under these conditions, the projection of eqs.(3.3) and (3.4) on the direction of $\boldsymbol{q}_n(t^o+t)$

gives:

$$\dot{\boldsymbol{q}}_n(t^o + t) = -|\boldsymbol{v}| \cdot \cos(\alpha_n(t^o)) \cdot \widehat{\boldsymbol{u}} \tag{3.5}$$

$$\ddot{\boldsymbol{q}}_n(t^o + t) = \boldsymbol{0} \tag{3.6}$$

where $\widehat{\boldsymbol{u}} = \dfrac{\boldsymbol{q}_n(t^o + t)}{|\boldsymbol{q}_n(t^o + t)|}$ is the unitary vector on the direction of $\boldsymbol{q}_n(t^o + t)$.
Consequently, $|\dot{\boldsymbol{q}}_n(t^o + t)|$ is constant for a small time interval of duration t s and the time-varying norm of the pathlength vector $|\boldsymbol{q}_n(t^o + t)|$ can be expressed as follows:

$$|\boldsymbol{q}_n(t^o + t)| = |\boldsymbol{q}_n(t^o)| - |\boldsymbol{v}| \cdot \cos(\alpha_n(t^o)) \cdot t. \tag{3.7}$$

Combining eqs.(3.1) and (3.7), the emission time is obtained from the reception time by

$$t = \left(t'_n - \frac{|\boldsymbol{q}_n(t^o)|}{c}\right) \cdot \left(\frac{c}{c - |\boldsymbol{v}| \cdot \cos(\alpha_n(t^o))}\right) \tag{3.8}$$

and eq.(3.2) becomes

$$y_n(t^o + t'_n) = \rho_n \cdot s_e\left(t^o + \left[t'_n - \frac{|\boldsymbol{q}_n(t^o)|}{c}\right] \cdot \left[\frac{c}{c - |\boldsymbol{v}| \cdot \cos(\alpha_n(t^o))}\right]\right). \tag{3.9}$$

Regardless of the effects related to the amplitude scale factor, eq.(3.9) describes clearly both the shift and the stretch of the time variation of the received signal with respect to the time variation of the emitted signal. The shift transformation is due to the sound propagation distance from the aircraft to the receiver and is defined here as:

$$\Delta T_n(t^o) = \frac{|\boldsymbol{q}_n(t^o)|}{c} \tag{3.10}$$

From fig.3.1, it can be seen that vector $\boldsymbol{q}_n(t^o)$ is equivalent to the resulting vector $\boldsymbol{r}_n - \boldsymbol{p}(t^o)$. As all the receiver positions $\boldsymbol{r}_n$ $\forall n \in \{1, ..., N\}$ are known, the prior knowledge of an initial aircraft position $\boldsymbol{p}(t^o)$ allows the computation of all $\Delta T_n(t^o)$ from

$$\Delta T_n(t^o) = \frac{|\boldsymbol{r}_n - \boldsymbol{p}(t^o)|}{c}. \tag{3.11}$$

Then, the signal received at each microphone can be synchronized so that the origin of all of them corresponds to a common position of the aircraft in flight. The synchronized set of signals are defined as follows:

$$x_n(t'_n) = y_n(t^o + t'_n + \Delta T_n(t^o)) \qquad \forall n \in \{1, ..., N\}. \tag{3.12}$$

Now, combining eqs.(3.9) and (3.12), the relation between the synchronized signals and the emitted signal is:

$$x_n(t'_n) = \rho_n \cdot s_e \left(t^o + \left[\frac{c}{c - |\boldsymbol{v}| \cdot \cos(\alpha_n(t^o))} \right] \cdot t'_n \right). \tag{3.13}$$

It has to be noted that the same portion of all synchronized signals, $x_n(t')$ for $0 \leq t' \leq \Delta t$ $\forall n \in \{1, ..., N\}$, coincide at the origin with the same emitted signal but do not correspond exactly to the same emitted portion of signal. Each synchronized signal at the time $t' = \Delta t$ corresponds to the emitted signal at time $t^o + \frac{c}{c - |v| \cdot \cos(\alpha_n(t^o))} \cdot \Delta t$ which is different for each microphone location due to its dependence on α_n. However, this fact can be disregarded assuming that the aircraft velocity is constant during Δt and that $\left| \boldsymbol{p} \left(\max_n \left(\frac{c}{c - |v| \cdot \cos(\alpha_n(t^o))} \cdot \Delta t \right) \right) - \boldsymbol{p}(t^o) \right|$, which is the maximum change in the position of the aircraft during Δt among the position changes of the aircraft with respect to all receivers, is much smaller than $|\boldsymbol{q}_n|$.

The time scale coefficient in eq.(3.13) is the absolute Doppler stretch denoted here by

$$\delta f_n = \frac{c}{c - |\boldsymbol{v}| \cdot \cos(\alpha_n(t^o))}. \tag{3.14}$$

The frequency spectrum received by a microphone n can thus be expressed in terms of the emitted frequency spectrum by

$$X_n(f \cdot \delta f_n) = e^{j \cdot 2\pi \cdot f \cdot t^o} \rho_n \cdot S_e(f). \tag{3.15}$$

3.1.2 Doppler effect and aircraft localization

The signals received at each microphone location are time and frequency stretched with respect to the radiated signal due to the Doppler effect. As a consequence, the signals received by a pair of microphones are time and frequency stretched with respect to each other. The scale factor between both received signals is named relative Doppler stretch in this thesis and it can be expressed as a function of the aircraft position and velocity as follows.

Geometric relations in fig.3.1 lead to the following equation:

$$|\boldsymbol{v}| \cdot \cos(\alpha_n(t^o)) = \frac{\boldsymbol{v} \cdot \boldsymbol{q}_n}{|\boldsymbol{q}_n|} \tag{3.16}$$

where the product $\boldsymbol{v} \cdot \boldsymbol{q}_n$ is the scalar product of the aircraft velocity and the pathlength vector between the aircraft and receiver n. Using this expression and substituting $\boldsymbol{q}_n$ for $\boldsymbol{r}_n - \boldsymbol{p}$, the absolute Doppler stretch, δf_n, of the synchronized signal $x_n(t')$ in eq.(3.13) with respect to the emitted signal can be written as:

$$\delta f_n = \frac{c}{c - \dfrac{\boldsymbol{v} \cdot (\boldsymbol{r}_n - \boldsymbol{p})}{|\boldsymbol{r}_n - \boldsymbol{p}|}} \tag{3.17}$$

Combining eq.(3.17) for receivers m and n, the relative Doppler stretch δf_{mn} is:

$$\delta f_{mn} = \frac{c - \dfrac{\boldsymbol{v} \cdot (\boldsymbol{r}_n - \boldsymbol{p})}{|\boldsymbol{r}_n - \boldsymbol{p}|}}{c - \dfrac{\boldsymbol{v} \cdot (\boldsymbol{r}_m - \boldsymbol{p})}{|\boldsymbol{r}_m - \boldsymbol{p}|}}. \tag{3.18}$$

This expression describes the relation between the relative Doppler stretch and the aircraft position and velocity. Six scalar unknowns appear in eq.(3.18), $\boldsymbol{p} = (p_x, p_y, p_z)$ and $\boldsymbol{v} = (v_x, v_y, v_z)$, at any given time. Writing eq.(3.18) for at least six microphone pairs six equations with six unknowns are stated. Then, the aircraft position and velocity can be calculated by solving this non-linear equation system with prior computation of the six relative Doppler stretches.

3.1.3 Computation of the relative Doppler stretch

As seen in section 3.1.1, the sound signals at a given receiver are delayed and time (and frequency) stretched with respect to the signals at the other receivers. Kelly and Wishner introduced in ref.[28] the wideband cross-ambiguity function which provides the time delay τ_{mn} and the relative time stretch δf_{mn} between two different signals y_m and y_n received by microphones m and n. The ambiguity function applied to these signals is defined as follows:

$$\chi(\tau, \sigma) = \sqrt{\sigma} \int_{-\infty}^{\infty} y_m(t) \cdot y_n(\sigma \cdot (t - \tau)) \mathrm{d}t. \tag{3.19}$$

The ambiguity function reaches its absolute maximum for $\tau = \tau_{mn}$ and $\sigma = \sigma_{mn}$. However, difficulties arise from the detection of the maximum peak in a two-dimensional domain [29] and different techniques for wideband correlation processing have been presented in the literature as those based on the wavelet theory [30, 31]. For the present method, the use of the two dimensional ambiguity function is avoided as both signals in eq.(3.19) are synchronized (section 3.1.1) and they are not time delayed. Therefore the delay variable τ is known, $\tau = 0$, and the following one-dimensional version of the ambiguity function (3.19) is used to obtain the relative time stretch by detecting its maximum:

$$\chi(\sigma) = \sqrt{\sigma} \int_{-\infty}^{\infty} y_m(t) \cdot y_n(\sigma \cdot t) \mathrm{d}t. \tag{3.20}$$

From a generalized point of view, eq.(3.20) describes the degree of similarity between two functions defined on a relative stretched domain. Thus, this version of the ambiguity function is not time domain restrictive and the two modules $|X_m(f)|$ and $|X_n(f)|$ of the frequency spectra of the synchronized signals $x_m(t')$ and $x_n(t')$ may be used as well. For a more coherent notation, σ can be rewritten as a relative frequency stretch δf and eq.(3.20) becomes:

$$\chi(\delta f) = \sqrt{\delta f} \int_{-\infty}^{\infty} |X_m(f)| \cdot |X_n(\delta f \cdot f)| \, \mathrm{d}f. \tag{3.21}$$

Therefore, the maximum value of $\chi(\delta f)$ will correspond to $\delta f = \delta f_{mn}$, the value of the relative Doppler stretch between two received signals after being synchronized.

The result of using the 1D ambiguity function on two different signals is the reduction of the effect of the background noise in the localization process, since it is considered that the measurement points are not close together and thus their background noise is independent and uncorrelated. In ref.[27], the experimental results presented show no relevant differences in the localization errors obtained for the cases of +6dB and +3dB values of signal-to-noise ratio (SNR), and the case assuming no background noise.

3.1.4 Iterative source localization

The only requirement of the acoustic method described in the present thesis is a prior knowledge of the sound source position $\boldsymbol{p}(t^o)$ at some time instant t^o. The sound source

considered here is an aircraft. For simplicity, the known position could be either the takeoff position or the final position when the aircraft is landing. By means of a surveillance camera on the track or another aircraft-position sensor, these specific positions may not be difficult to obtain. The aircraft localization can be done during both takeoff and landing procedures. Assuming that the takeoff position and time, $\boldsymbol{p}(t^o)$ and t^o, are known, the signals received by the acoustic sensors can be all synchronised by means of the technique explained in section 3.1.1. Then, from each synchronised signal a portion of duration Δt is considered, $x_n(t')$ for $0 \leq t' < \Delta t \ \forall n$, and is transformed to the frequency domain $X_n(f)$ by means of the Fourier Transform. Then, the one-dimensional version of the ambiguity function (3.21) can be calculated for the spectrum of a reference receiver (without loss of generality, let m be fixed at $m = 1$) and the spectrum of at least six different receivers $n \in \{2, ..., 7\}$ in order to compute the six relative Doppler stretches δf_{1n}. The relation expressed in eq. (3.18) between δf_{1n} for $n \in \{2, ..7\}$ and the position and velocity of the aircraft leads to a non-linear system of six equations and six unknowns. The solution of this system provides an estimate of the aircraft position $\boldsymbol{p}$ and velocity $\boldsymbol{v}$ assigned to the time $t^o + \Delta t/2$. After this first iteration, the aircraft position obtained, $\boldsymbol{p}(t^o + \Delta t/2)$, becomes the initial position needed to be known to synchronize the time signals at each receiver location. The location algorithm can then be executed all over again to obtain, at each iteration k, the aircraft position and velocity, $\boldsymbol{p}^k = \boldsymbol{p}(t^o + k \cdot \Delta t/2)$ and $\boldsymbol{v}^k = \boldsymbol{v}(t^o + k \cdot \Delta t/2)$. The block diagram in fig.3.2 summarizes the aircraft localization method described in this thesis.

3.2 Implementation

3.2.1 Parameters

The parameters to be chosen for the implementation of the acoustic localization method described in section 3.1 are:

- f_m, the sampling rate of the signals to be registered, received by all seven sensors
- Δt, the time interval of the signal portions used at each iteration of the location algorithm.

The sampling rate has to be chosen by prior observation of the main frequency content of the sound source spectrum. The value of f_m must be greater than the Nyquist rate

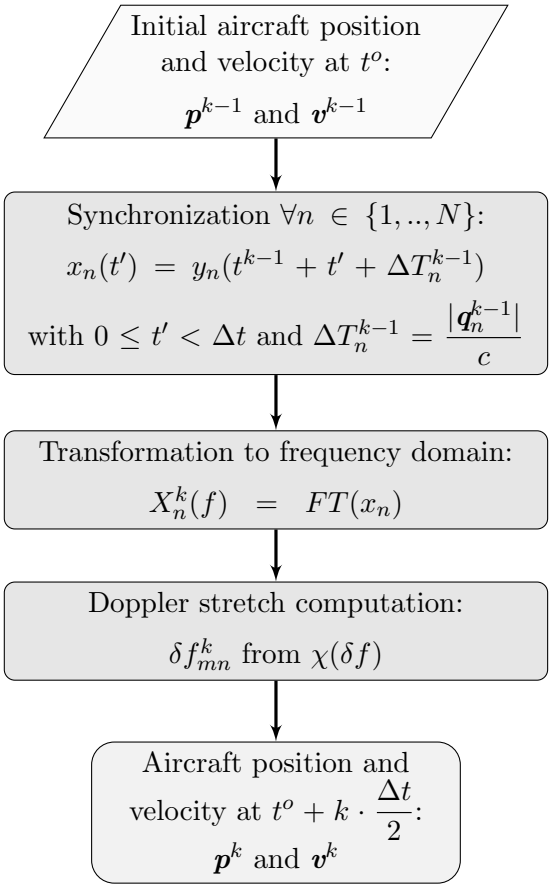

FIGURE 3.2: Block diagram of the k^{th}-iteration of the aircraft localization algorithm.

which is twice the bandwidth upper limit of the main content of the frequency spectrum in order to avoid aliasing. Moreover, since the method described here deals with a correlation between frequency spectra received by different microphones, the sampling rate will determine the frequency limit to be up to the Nyquist frequency $f_m/2$.

Three important conditions concerning the value of Δt must be fulfilled.

- The first one is that $|\boldsymbol{v}| \cdot \Delta t << |\boldsymbol{q}_n(t^o)|$ and can be accomplished by selecting small values of Δt.
- The second is that during Δt s, the velocity $\boldsymbol{v}$ must be assumed constant which is also possible for small values of Δt.
- The third and last condition is that Δt should be large enough to obtain an acceptable frequency resolution Δf when the Fourier Transform of the synchronised signals is computed.

If one of the first two conditions is not satisfied, $\boldsymbol{v}\cdot\cos(\alpha_n(t^o+t'))$ can not be considered constant for $0 \leq t' \leq \Delta t$ and then the variation of the relative Doppler stretch is not be negligible. The method would not be valid since it deals with instantaneous Doppler stretches. Therefore, a compromise value of Δt must be selected in each application of the method.

3.2.2 Calculation of relative Doppler stretch

The following discrete version of the one-dimensional ambiguity function (3.21) is calculated to compute the relative Doppler stretches δf_{1n}, $n \in \{2,..,7\}$:

$$\chi(k\cdot\Delta\delta f) = \frac{\sqrt{k\cdot\Delta\delta f}}{L+1}\sum_{l=0}^{L}|X_1(l\cdot\Delta f)|\cdot|X_n((k\cdot\Delta\delta f)\cdot(l\cdot\Delta f))| \tag{3.22}$$

where $\Delta\delta f$ can be understood as a Doppler stretch resolution, $k \in \mathbb{N}$ and

$$L = \begin{cases} \left\lfloor \dfrac{f_m/2\cdot k\cdot\Delta\delta f}{\Delta f} \right\rfloor & \text{if } \delta f < 1, \\ \left\lfloor \dfrac{f_m/2}{\Delta f} \right\rfloor & \text{if } \delta f \geq 1. \end{cases}$$

An adequate range of Doppler stretches for which the discrete ambiguity function is calculated and which is valid during the whole flight procedure of an aircraft is determined by observing the expression of δf_{1n} in eq.(3.18) rewritten as

$$\delta f_{1n} = \frac{c-|\boldsymbol{v}|\cdot\cos(\alpha_n(t^o))}{c-|\boldsymbol{v}|\cdot\cos(\alpha_1(t^o))}. \tag{3.23}$$

Thus, the following inequality holds

$$\frac{c-|v_{max}|}{c+|v_{max}|} \leq \delta f_{mn} \leq \frac{c+|v_{max}|}{c-|v_{max}|}, \tag{3.24}$$

where $|v_{max}|$ is the possible maximum speed that the aircraft to be located can reach. Therefore, the integer k in eq.(3.22) has the following lower and upper limits

$$\left\lceil \frac{c-|v_{max}|}{c+|v_{max}|}\cdot\frac{1}{\Delta\delta f} \right\rceil \leq k \leq \left\lfloor \frac{c+|v_{max}|}{c-|v_{max}|}\cdot\frac{1}{\Delta\delta f} \right\rfloor. \tag{3.25}$$

Concerning the spectra in eq.(3.22), note that the upper limit of $X_n(l \cdot \Delta f)$ for all $n \in \{1, .., 7\}$ is

$$\lfloor \frac{f_m/2 \cdot}{\Delta f} \rfloor \cdot \Delta f.$$

If the frequency axes of X_n is stretched by a factor $k \cdot \Delta\delta f < 1$, its new upper frequency limit is smaller and thus the common upper frequency of X_1 and X_n is

$$\left\lfloor \frac{f_m/2 \cdot k \cdot \Delta\delta f}{\Delta f} \right\rfloor,$$

which is lower than $\lfloor \frac{f_m/2 \cdot}{\Delta f} \rfloor \cdot \Delta f$. This is the reason why L in eq.(3.22) changes its value as a function of δf. Moreover, both spectra in eq.(3.22) have to be sampled at the same frequency values. To that aim, the stretched spectrum $X_n((k \cdot \Delta\delta f) \cdot (l \cdot \Delta f))$ is linearly interpolated and thus sampled at the same frequencies as $X_n(l \cdot \Delta f)$.

3.2.3 Calculation of aircraft position

To obtain the aircraft position and speed, the system of non-linear equations (3.18) for δf_{1n}, $n \in \{2, .., 7\}$ is treated as a least squares problem expressed as follows,

$$\min_{(\boldsymbol{p}, \boldsymbol{v}) \in I} \sum_{n=2}^{N} \left(\delta f_{1n} - \frac{c - \dfrac{\boldsymbol{v} \cdot (\boldsymbol{r}_n - \boldsymbol{p})}{|\boldsymbol{r}_n - \boldsymbol{p}|}}{c - \dfrac{\boldsymbol{v} \cdot (\boldsymbol{r}_1 - \boldsymbol{p})}{|\boldsymbol{r}_1 - \boldsymbol{p}|}} \right)^2 \tag{3.26}$$

where $I \subseteq \mathbb{R}^6$. The present least squares problem is solved by means of genetic algorithms. Holland's original genetic algorithm described in ref.[32], the simple genetic algorithm (SGA), has been used because of its simplicity and efficiency. The definition of the search space $I \subseteq \mathbb{R}^6$ depends on the aircraft position calculated in a previous iteration and on the minimum and maximum possible values of aircraft speed. Therefore, the solution of the problem formulated in the kth iteration of the location algorithm $(\widehat{p_x^k}, \widehat{p_y^k}, \widehat{p_z^k}, \widehat{v_x^k}, \widehat{v_y^k}, \widehat{v_z^k})$ is searched in the interval $I = [I_x, I_y, I_z, I_{v_x}, I_{v_y}, I_{v_z}] \subseteq \mathbb{R}^6$, where

$$I_u = \left[\widehat{p_u^{k-1}} - |v_{max,u}| \cdot \frac{\Delta t}{2}; \widehat{p_u^{k-1}} + |v_{max,u}| \cdot \frac{\Delta t}{2} \right] \text{ and } I_{v_u} = [v_{min,u}; v_{max,u}]$$

where $u = x, y, z$ and $k > 0$. Once the aircraft position and speed at $t_o + k \cdot \frac{\Delta t}{2}$ are obtained, the pair of values $\dfrac{t^k}{2}$ and $\widehat{p^k}$ is used to synchronize the signals again and the whole calculation procedure starts all over.

Chapter 4

Computer simulation

The acoustic localization method has been implemented by using the programming software Matlab. The present chapter deals with the computer simulations carried out considering two different models of sound propagation from the aircraft to the receivers. Section 4.1 aims at assessing the performance of the different steps of the acoustic method on the sound source localization. With the purpose to isolate the influence of each step, section 4.1 considers a simple sound propagation model assuming a lossless medium. Section 4.2 focusses on the method application to aircraft localization. To that aim, and because of large distances between the aircraft and receivers, the atmospheric attenuation influencing the aircraft noise propagation needs to be considered. Therefore, section 4.2 introduces a sound propagation model for a homogeneous but non lossless medium. Note that the directivity of the source would be a relevant factor only if it varies as a function of the frequency. Under these circumstances, the magnitude of the frequency spectra received by the set of microphones may not be anymore a frequency stretched version of each other. For jet commercial aircrafts, the influence of the directivity is clearly dependent on the emitted frequency. For light aircrafts and helicopters, the frequency dependence is expected to be lower and thus, their directivity would not influence significantly on the acoustic localization method. In this thesis the aircraft is modeled as an omnidirectional source, leaving the study of the influence of the directivity for further developments.

4.1 Omnidirectional source in a lossless medium

The aim of this section is to evaluate the performance of two of the main tools of the method: the genetic algorithm used to solve the location problem, and the 1D ambiguity function used to estimate the relative Doppler stretch. Also the influence of the positions of the receivers and the uncertainty of the source initial position on the accuracy of the method are discussed. The present section is organized as follows. Section 4.1.1 describes the implementation of the acoustic method in the case of considering a lossless medium. The acoustic method setup, the sound propagation model and the parameters used by the method are introduced. Section 4.1.2 presents the results obtained from the computer simulation.

4.1.1 Description of the computer simulation

4.1.1.1 Setup

The setup involves seven microphones distributed over a region of interest around an hypothetical airport. Figure 4.1 shows the positions of the receivers with respect to the aircraft flight paths that has been used for the simulation. Table 4.1 lists the coordinates of the receivers with respect to the origin of coordinates, which is at the position where takeoff starts at the time of liftoff.

TABLE 4.1: Position of the seven receivers $n \in \{1, ..., 7\}$ with respect to the origin of coordinates

n	1	2	3	4	5	6	7
r_{nx} [m]	2800	720	1040	3240	4760	6640	6680
r_{ny} [m]	-320	1120	-1028	1360	0	-800	1000

Two aircraft takeoff-climb-out paths has been considered. Both are based on the takeoff-climb-out data provided in the database of the Integrated Noise Model (INM) from the Federal Aviation Administration (FAA) for a Boeing 737-400. The original data extracted from the software database are the height and the speed of the aircraft for a discrete set of ground distances from the takeoff point. The INM provides data for various segments of the path with the engines operating at different power settings to allow initiation of thrust cutback at appropriate distances from start. The continuous path of the aircraft has been reconstructed by assuming a straight-line motion with a constant acceleration between two consecutive known positions. The direction of the

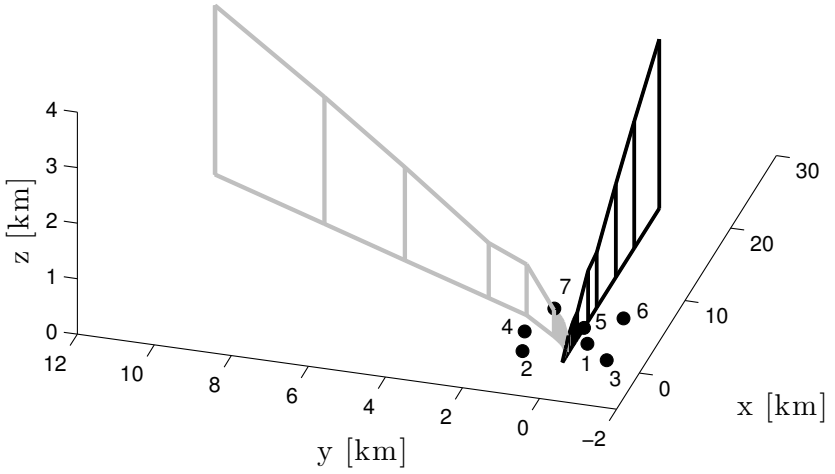

FIGURE 4.1: Flight path geometry and receiver locations. In bold black, the straight trajectory is parallel to the x-axis from liftoff at $x = 0$, $y = 0$, $z = 0$; in gray a turning trajectory. The numbered dots designates the positions of the seven receivers. For illustration, the x-axis is shown displaced -2 km from the origin of coordinates and the z-axis is displaced +12 km from the origin.

aircraft velocity is assumed to change instantaneously at the beginning of each segment. One of the trajectories is in the xz-plane and thus the y-coordinate of the aircraft position is $p_y = 0$ at any time (black straight trajectory in fig.4.1). The other is a turning path following the curvature of the CLE1E departure path from the Barcelona Airport, El Prat. Figure 4.2 shows the acceleration vector of the aircraft as a function of time after liftoff. Note that there is negligible difference in the acceleration and airspeeds of the two flight paths.

4.1.1.2 Aircraft sound-propagation model

For the purpose of the computer simulation, the sound from an aircraft is assumed to be equivalent to that radiated from a monopole sound source represented by a pulsating sphere at a point on the flight path. The source sound power is a function of the acoustic strength, Q, of the pulsating sphere. Source strength has the unit of cubic metres per second for the rate of change for the volume displacement.

Figure 4.3 shows the frequency spectrum of the aircraft's acoustic strength Q used in the simulations. The estimate of source strength has been obtained from a measurement

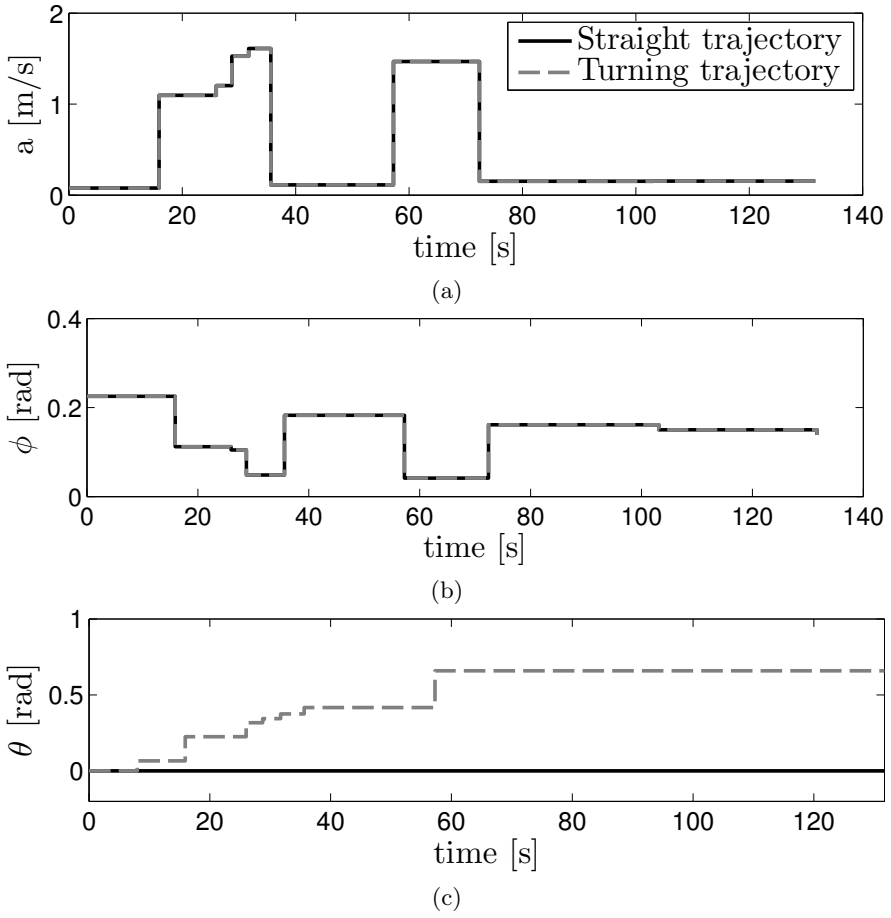

FIGURE 4.2: a) Modulus of the aircraft acceleration vector, b) azimuth angle of the aircraft acceleration vector (counter-clockwise relative to the x-axis in fig.4.1), and c) elevation angle of the aircraft acceleration vector as a function of time (clock-wise relative to the z-axis)

of the sound-pressure spectrum from a 737-400 during a flyby and at the time of CPA. The measured spectrum is propagated back over the pathlength to the location of the aircraft. The sound-pressure spectrum at the source provides an estimate of the average sound intensity over the surface of the sphere which equals the sound power and thus the source strength can be derived. Because the aircraft was at the closest point of approach of the receiver, the Doppler effect on the frequency spectrum is considered negligible. For simplicity, the frequency spectrum of the strength of the aircraft is assumed to be constant along the trajectory regardless of the engine operating conditions. The time function of the source strength $Q(t^*)$ has been reconstructed from the spectrum in fig.4.3.

Figure 4.4 shows the geometry of the aircraft flight path at an instantaneous position where $\boldsymbol{p}(t)$ is the position vector of the aircraft to the origin of coordinates, $\boldsymbol{v}(t)$ is the

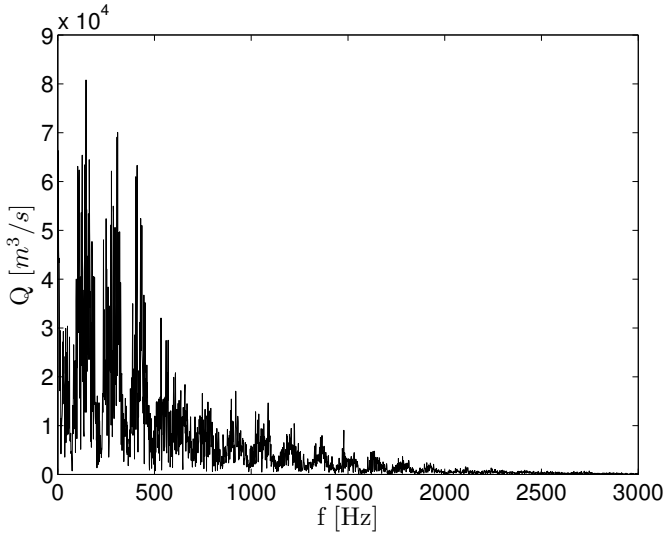

FIGURE 4.3: Frequency spectrum of the aircraft strength $Q(f)$

instantaneous velocity vector, $\boldsymbol{r}_n$ is the position vector from the origin to receiver n, and $\boldsymbol{q}_n(t)$ is the pathlength vector from the source to receiver n.

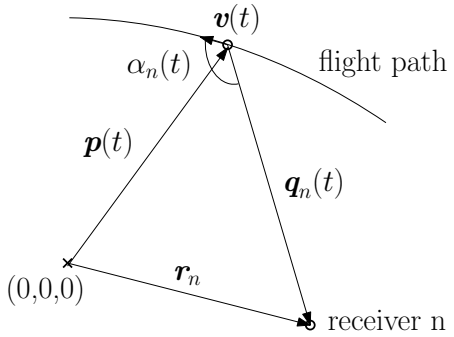

FIGURE 4.4: Flight path geometry

The sound signal emitted by the aircraft at the time t has to travel over the pathlength $\boldsymbol{q}_n(t)$, and therefore reaches receiver n at time

$$t'_n = t + \frac{|\boldsymbol{q}_n(t)|}{c}. \tag{4.1}$$

From now on, t is be referred as the emission time and t'_n as the receiver time.

In the computer simulation the aircraft is considered to be a moving point source in a lossless medium of constant temperature. Therefore the relation between the sound-pressure signal at receiver n and the strength of the source is given by ref.[33] as

$$y_n(t'_n) = \left[\frac{Q(t)}{4\pi|\boldsymbol{q}_n(t|)}\right] \cdot \left[\frac{c}{c - |\boldsymbol{v}| \cdot \cos(\alpha_n(t))}\right]. \tag{4.2}$$

The first term on the right in eq.(4.2) describes the pressure field generated by a fixed non-moving point source of strength $Q(t)$. The second term on the right indicates that for a moving point source, the perturbations in the sound pressure when it moves towards a receiver are higher than when it moves away from a receiver.

Combining eqs.(4.1) and (4.2) a mathematical function for the signal received at microphone n is obtained as a function of emission time t

$$y_n\left(t + \frac{|\boldsymbol{q}_n(t)|}{c}\right) = \left[\frac{Q(t)}{4\pi|\boldsymbol{q}_n(t)|}\right] \cdot \left[\frac{c}{c - |\boldsymbol{v}| \cdot \cos(\alpha_n(t))}\right]. \tag{4.3}$$

With the aircraft flight path, the time evolution of its speed, and its emitted source strength as inputs, eq.(4.3) allows to simulate the spectrum of the sound pressure signal at each receiver location.

4.1.1.3 Implementation

Initialization

The only requirement of the location method is an initial position of the aircraft $\boldsymbol{p}^0$ at some time t^o. For the computer simulation presented in this thesis, $\boldsymbol{p}^0 = (0, 0, 0)$ m is assumed to be the liftoff position and $t^o = 0$ s is considered to be the time at which this position is reached. This initial position allows the synchronization of all received signals assuming c=340 m/s (section 3.1.1) such that the origin of all synchronized signals corresponds to the signal emitted at $t^o = 0$ s.

Parameters

The sampling rate is chosen by observing the frequency content of a standard aircraft spectrum. The spectrum is concentrated from 125Hz to 2500Hz (see ref.[34]) and thus, the sampling rate selected is 6000 samples per second following the criterion stated in section 3.2.

Concerning to the signal portions, Δt is set to 0.5 s which let the frequency resolution of $X_n(f)$ to be 2 Hz. Moreover, the maximum variation of δf_{1n} for the distributed microphones of Table 4.1 is less than 5%. So, the assumption of the

Doppler stretches to be constant during Δt is acceptable.
Since Δt is 0.5 s, the aircraft in flight is located every $\dfrac{\Delta t}{2} = 0.25$ s.

Calculation of relative Doppler stretch

To speed up the calculations of the 1D ambiguity function and with the exception of the first iteration of the location method, the calculation is performed only for the range $k\Delta\delta f \in [\delta f_{1n}(t^o - \frac{\Delta t}{2}) - 0.05; \delta f_{1n}(t^o - \frac{\Delta t}{2}) + 0.05]$ where 0.05 is the maximum possible variation of δf_{1n} in an interval of $\Delta t = 0.5$ s. The Doppler stretch resolution $\Delta\delta f$ is set to 10^{-4} which correspond to the 0.2% of the maximum variation 0.05. The value of $k\Delta\delta f$ for which the maximum of $\chi(k \cdot \Delta\delta f)$ is reached, is assigned to δf_{1n}.

Calculation of aircraft position

The employed genetic algorithm uses the parameters specified in ref.[35] as appropriate for solving the system of equations (3.18). In the present problem, six unknowns are searched and thus the parameter NVAR of the SGA is set to 6. The maximum number of generations permitted has been 3500. Concerning the search space, the minimum and maximum value of the aircraft speed have been 0 m/s and 150 m/s respectively.

4.1.2 Results

The results obtained from the described method are given in terms of the x, y, z coordinates of the position along the flight path as a function of time. Figures 4.5 and 4.6 show the estimated aircraft position $\widehat{p} = (\widehat{p_x}, \widehat{p_y}, \widehat{p_z})$ along with the theoretical position $p = (p_x, p_y, p_z)$ considering the straight and the turning trajectories from fig.4.1.

When the absolute errors of the three spatial coordinates have been increasing simultaneously during at least 12 iterations of the localization algorithm or equivalently 3 seconds of localization, the acoustic method is considered to be not accurate enough. For the straight trajectory, this happens at time $t = 54$ s after liftoff; at this instant the aircraft's theoretical position is $p = [5276, 0, 847]$ m. For the turning trajectory, it happens at $t = 62$ s after liftoff when the aircraft's theoretical position is $p = [5860, 1957, 941]$ m. Notice that both positions are inside the area covered by the sensor and almost at 1 km of altitude.

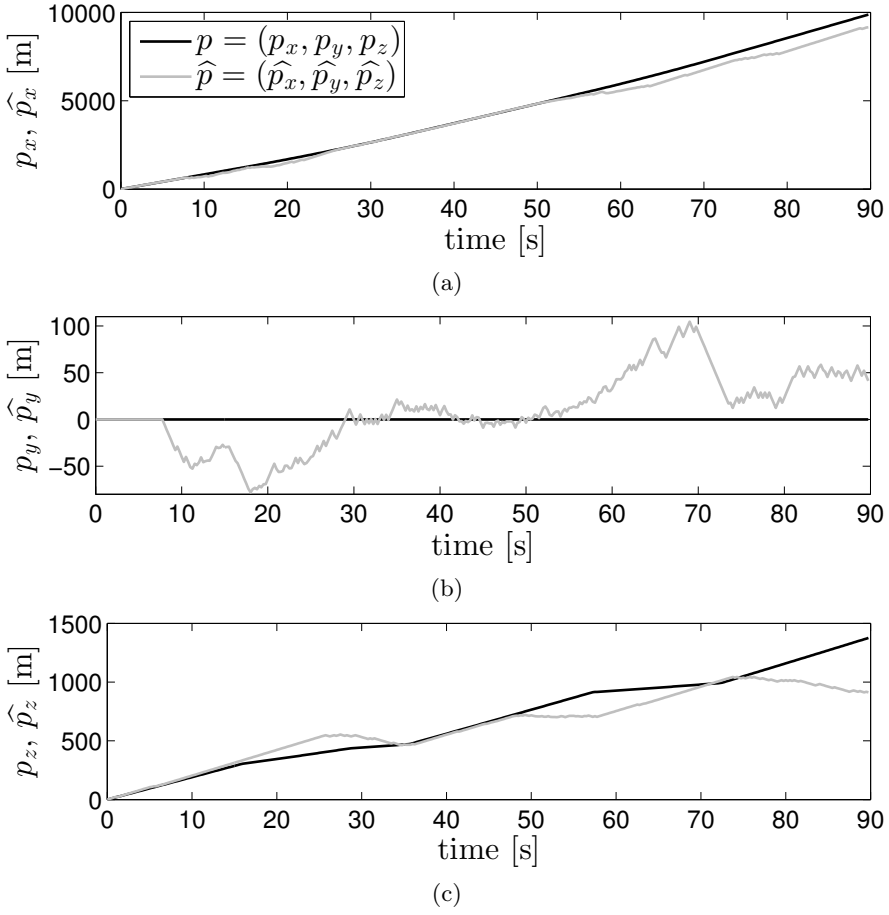

FIGURE 4.5: Theoretical and estimated aircraft positions for the straight trajectory of fig.4.1: a) refers to projections of the flight path on the x-axis, b) on the y-axis, and c) on the z-axis.

The errors in the estimated positions are listed in Table 4.2 for both trajectories. An error is defined here as a deviation from the theoretical flight path. The mean error has been calculated by means of

$$\widehat{Err}_u = \frac{\sum_{k=1}^{K} |\widehat{p}_u^k - p_u^k|}{K} \tag{4.4}$$

where p and $\widehat{p}$ are the theoretical and estimated aircraft positions, $u = x, y, z$ and K is the maximum number of executed iterations of the localization algorithm. The maximum errors for each spatial coordinate are evaluated for the time interval before the method clearly ceases to locate the aircraft, this is, at $t \in [0; 54]$ s and $t \in [0; 62]$ s for the straight and turning trajectory when the aircraft is up to 5.3 km and 6.2 km away from the origin of coordinates respectively.

The mean errors prove the generally good performance of the localization algorithm

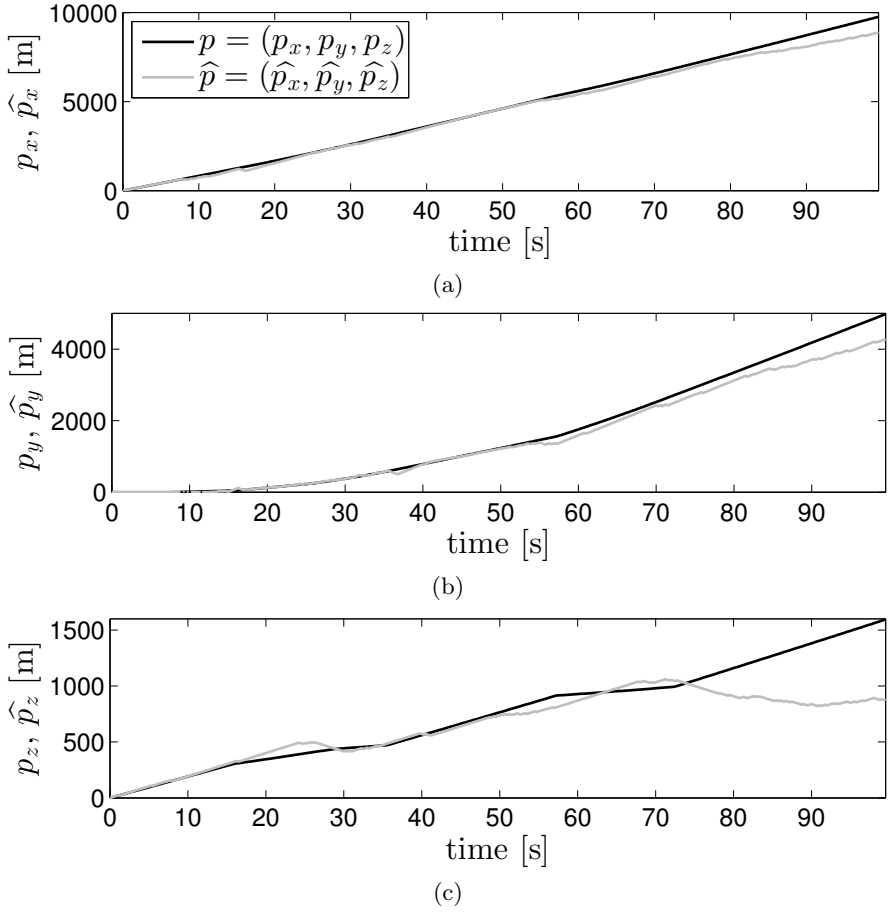

FIGURE 4.6: Theoretical and estimated aircraft positions for the turning trajectory of fig.4.1: a) refers to projections of the flight path on the x-axis, b) on the y-axis, and c) on the z-axis.

taking into account that for a Boeing 737-400, the length of the fuselage is 36.45 m and the wingspan is 28.88 m. However, the values of the maximum errors require detailed analysis to determine their possible causes. The next sections study the possible influences of the different steps of the algorithm on the results obtained. The results of the simulations are similar for both trajectories shown in fig.4.1. Therefore, only the results for the straight trajectory are considered further on.

The next sections organized as follows: section 4.1.2.1 explores the influence of the receiver's spatial distribution, section 4.1.2.2 evaluates the accuracy of the simple genetic algorithm used for the equation-system resolution, section 4.1.2.3 assesses the accuracy of the 1D ambiguity function, and finally, section 4.1.2.4 studies the method behavior under uncertainty of the source initial position.

TABLE 4.2: Evaluation of the maximum and mean error reached by each spatial coordinate x, y, z for time intervals $[0;54]$ s and $[0;62]$ s (the aircraft being up to 5.3 km and 6.2 km far from the origin of coordinates respectively) for the straight and turning trajectories from fig.4.1.

	u	$\max(Err_u)$ [m]	$\widehat{Err}_u$ [m]
Straight path	x	248.02	53.14
	y	77.95	19.11
	z	145.5	43.35
Turning path	x	238.7	68.75
	y	211.3	36.89
	z	105.5	33.51

4.1.2.1 Influence of the receiver positions

A relationship has been found between the receivers distribution and the point at which the method stops locating accurately the aircraft. This section tests different spatial configuration of the receivers that allow to assess the performance of the method and the accuracy on the Doppler stretches calculation. Nevertheless, it is not the aim of the section to provide an optimal distribution of the receivers.

The position of the receivers is directly related to the relative Doppler stretches by eq.3.18. Figure 4.7a shows the theoretical time evolution of the six relative Doppler stretches, δf_{1n} where $n \in \{2, ..., 7\}$, for the receiver positions given in Table 4.1. For $t > 54$ s (the aircraft being more than 5.3 km far from the origin of coordinates), the relative Doppler stretches of receivers 2, 3, 4, and 5 are similar and different from the relative Doppler stretches of 6 and 7 which are in turn similar. Therefore, it seems that when several relative Doppler stretches take approximatively the same value, the acoustic localization method is not able to determine reasonable values for the position of the aircraft. The same effect is observed in the time interval $t \in [20;35]$ s when only up to three clearly different values for the six relative Doppler stretches can be distinguished. To see if there is also, in this time interval, a direct relation between the receiver positions and the error of the location estimation, another spatial distribution of receivers has been tested. In the new spatial distribution, all receivers have the same coordinates as in Table 4.1 except receivers 5 and 7. Microphone number 5 is removed from below the flight path (note $r_{5y} = 0$ m) and microphone number 7 instead of being the farthest microphone from the origin (note $r_{7x} \geq r_{nx}$, $n \in \{1, .., 6\}$) is now located

closer. Their new coordinates are

$$r_5 = (6000, 4000, 0) \text{ m}$$
$$r_7 = (-500, 3000, 0) \text{ m}.$$

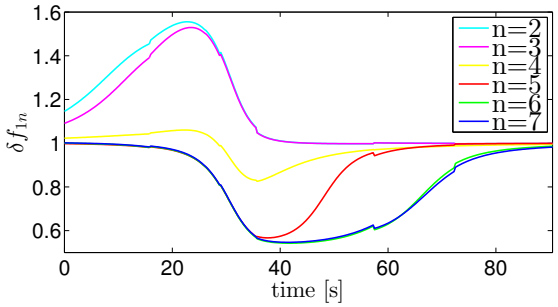

a) Microphones in distribution 1

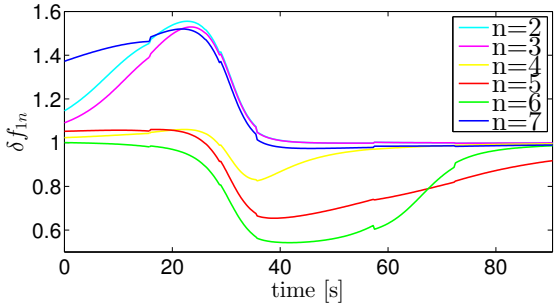

b) Microphones in distribution 2

FIGURE 4.7: Time evolution of the theoretical relative Doppler stretches δf_{1n}: a) for all receivers $n \in \{2, .., 7\}$ placed according to Table 4.1 (Distribution 1) and b) for the same receivers excepting receiver 5 which is located at (6000, 4000, 0) m and receiver 7 located at (-500, 3000, 0) m (Distribution 2).

Figure 4.7b shows that with this second receiver distribution at least four different values for the six relative Doppler stretches can be distinguished when $t \in [20; 35]$ s. Figure 4.8 representing the absolute value of the localization error $|\widehat{p_u} - p_u|$ of the three spatial coordinates $(u = x, y, z)$ for each receiver distribution confirms a better location estimation in the time interval $t \in [20; 35]$ s in case of receiver distribution 2. Therefore, the receiver positions clearly influence the accuracy of the aircraft location, and thus, to ensure an accurate and a longer functioning of the location algorithm, the time-varying relative Doppler stretches must remain as different as possible from each other. This condition can be achieved by choosing suitable receiver positions.

Despite of the enhanced localization, fig.4.8 shows a common location error increase when $t \in [20; 35]$ s for both receiver distributions. To assess where this increase lies,

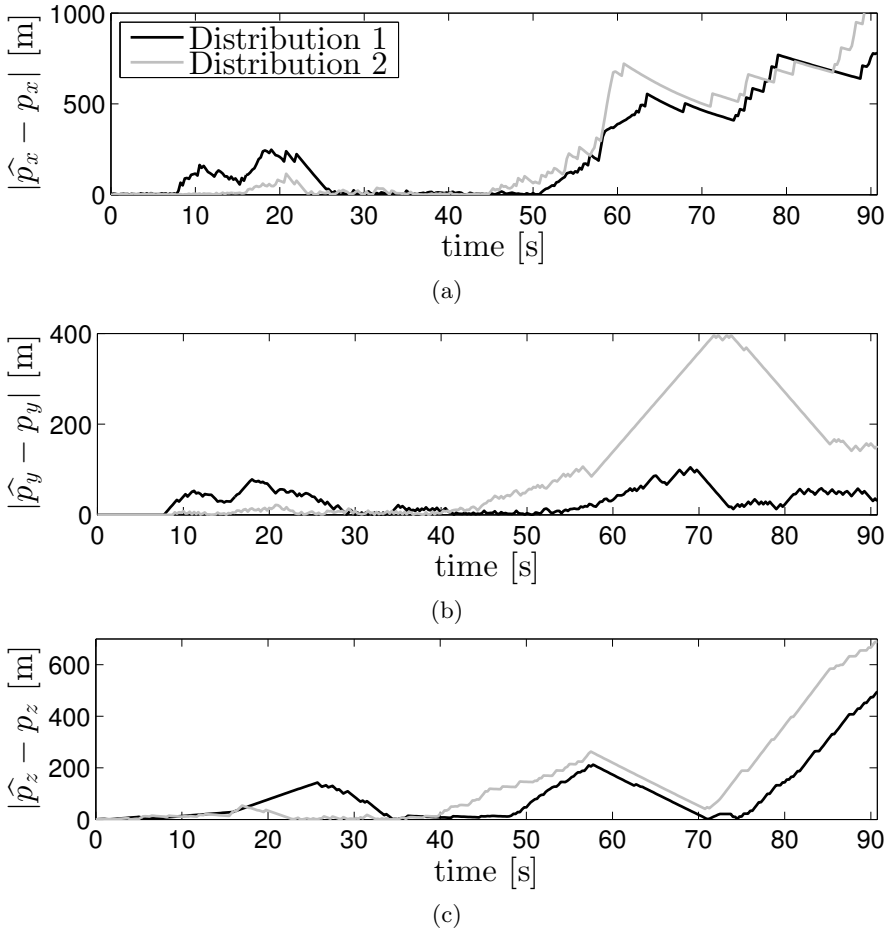

FIGURE 4.8: Absolute localization error for receivers in Table 4.1 (Distribution 1) and for the same receivers distribution except receiver 5 located at (6000, 4000, 0) m and receiver 7 located at (-500, 3000, 0) m (Distribution 2).

the time variation of the absolute error of the Doppler stretches for each receiver in the distribution 1 is represented in fig.4.9. This absolute error is the absolute value of the difference between the Doppler stretch obtained by means of the 1D ambiguity function (from now on named calculated Doppler stretches) and the Doppler stretch obtained by means of eq.(3.18) using the aircraft theoretical position (from now on named theoretical Doppler stretches). The error of the Doppler stretch for all receivers increases during the same time interval $t \in [20; 35]$ s. Moreover, this error increases as well for each particular receiver in different time intervals. The reason of these observations concerns the pathlength between each microphone and the sound source. Figure 4.10 shows the time evolution of the pathlength between the aircraft in flight and each receiver. Within $t \in [20; 35]$ s, the aircraft reaches the closest point of approach (CPA) to microphone 1, the microphone used as reference to calculate the relative Doppler stretches of all receivers. Furthermore, comparing figs.4.9 and 4.10 the particular increases of the error

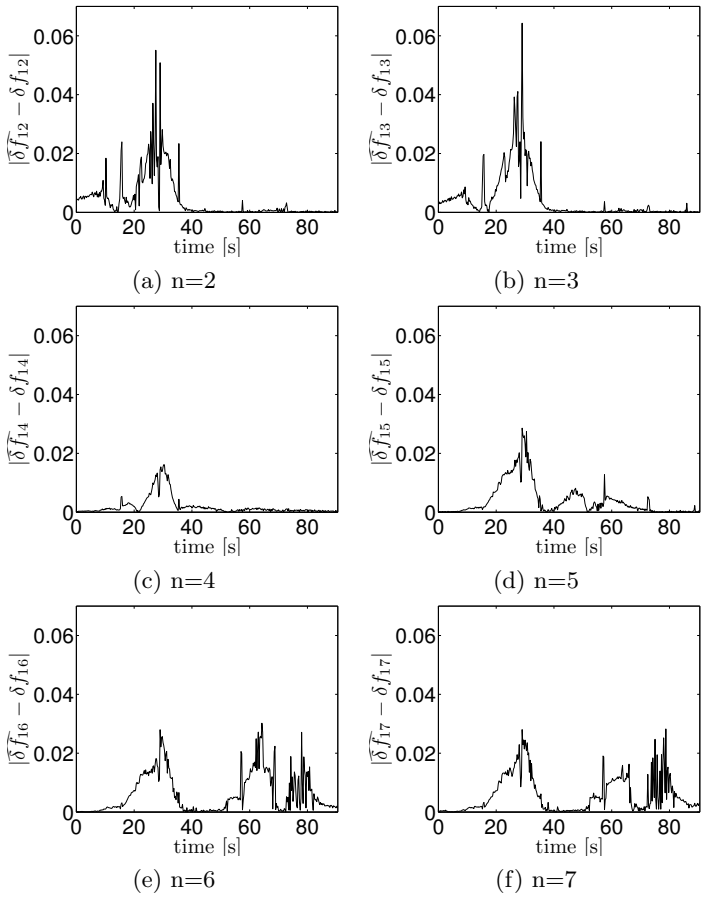

(a) n=2 (b) n=3

(c) n=4 (d) n=5

(e) n=6 (f) n=7

FIGURE 4.9: Absolute errors of the relative Doppler stretches for each receiver $n \in \{1, ..., 7\}$ distributed according to the coordinates in Table 4.1

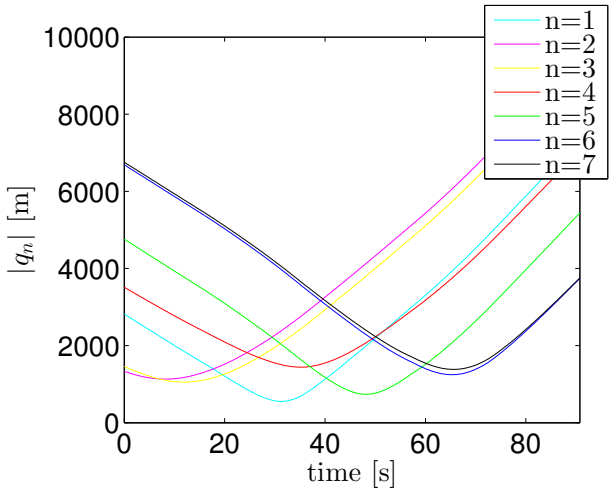

FIGURE 4.10: Time evolution of the distances between the aircraft and each receiver $n \in \{1, ..., 7\}$ distributed according to coordinates in Table 4.1

for each receiver occur around the time when the aircraft reaches the CPA to the receiver. Thus, is seems that it may be a relationship between the increase of the Doppler stretches error and the closest point of approach. To corroborate it, a new receiver distribution has been tested with all seven receiver positions different from those of Table 4.1. In this case, the CPA between the aircraft and each receiver occurs in different time intervals than the ones observed in fig.4.9.

The new coordinates of the receivers are listed in Table 4.3 taking into account that their z-coordinate r_{nz} is 0 since they are all distributed in the xy ground plane. Figure 4.11 shows the absolute error of the Doppler stretches for each receiver located by this third receiver distribution. An increase of the error for all receivers occurs in the time interval $[40; 60]$ s which indeed corresponds to the aircraft reaching the CPA of microphone 1 as showed in fig.4.12. Moreover, the particular increases of the Doppler stretches error can be as well associated to the minimum values of the pathlength $|q_n|$ for $n \in \{2, ..., 7\}$, i.e., when the aircraft approaches each of the receivers. Therefore, the estimation of the relative Doppler stretches losses accuracy when the aircraft reaches a receiver's CPA.

TABLE 4.3: Revised position of the receivers $n \in \{1, ..., 7\}$ with respect to the origin of coordinates

n	1	2	3	4	5	6	7
r_{nx} [m]	5000	720	2300	6000	7000	8000	-500
r_{ny} [m]	-320	500	-3500	2000	4000	-800	3000

An appropriate receivers distribution depends on the aircraft position, and therefore changes along an aircraft flight path. To ensure that an optimal set of relative Doppler stretches is always available along a flight path, more than seven receivers could be used. The idea is to develop an algorithm capable of choosing the optimal combination of six relative Doppler stretches among a larger mesh of receivers to solve eq.3.18 at every iteration of the calculation. The development of such an algorithm is outside the scope of the present thesis.

4.1.2.2 Accuracy of the genetic algorithm

To evaluate the error related to the method of resolution of the equation system in (3.18), the localization method has been tested using the theoretical relative Doppler stretches instead of the calculated ones in order to exclude the possible error associated with the ambiguity function. Also, the interval of search for the genetic algorithm has been defined using the previous theoretical position of the aircraft instead of the estimated

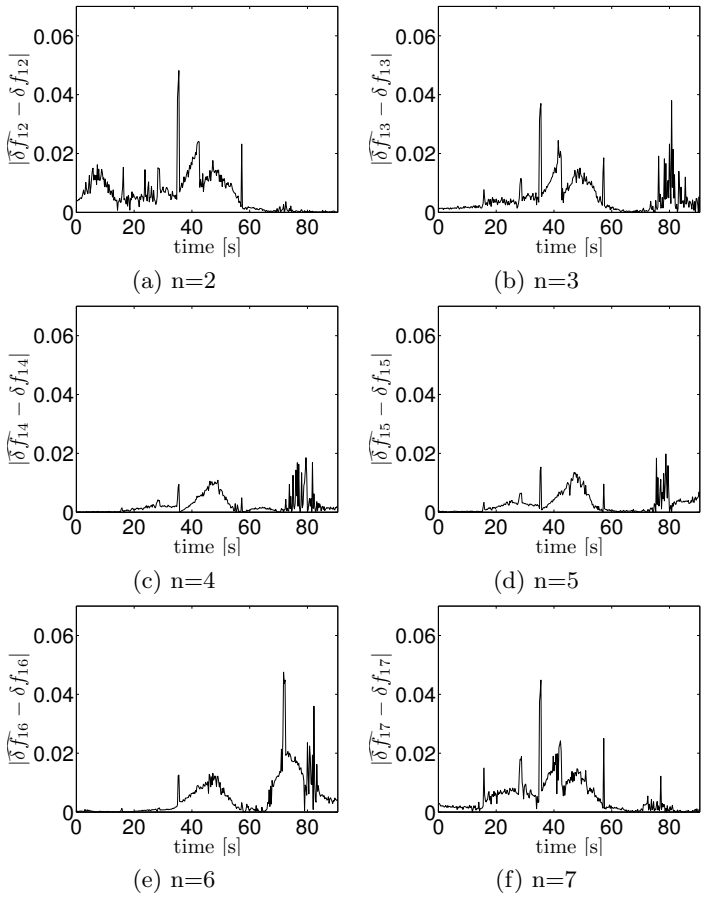

(a) n=2 (b) n=3

(c) n=4 (d) n=5

(e) n=6 (f) n=7

FIGURE 4.11: Absolute errors of the relative Doppler stretches for each receiver $n \in \{1, ..., 7\}$ distributed according to the coordinates in Table 4.3

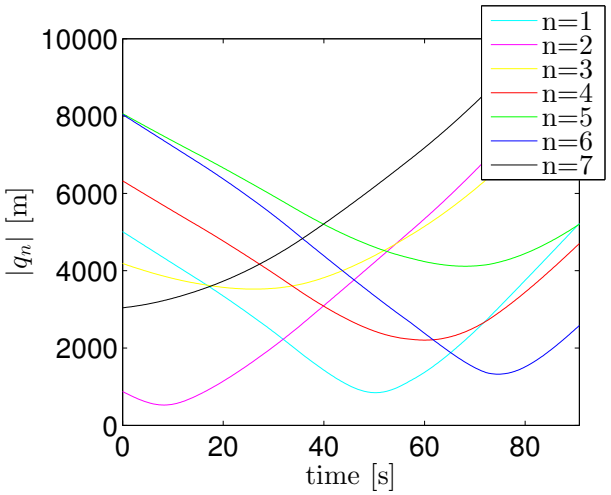

FIGURE 4.12: Time evolution of the distances between the aircraft and each receiver $n \in \{1, ..., 7\}$ distributed according to coordinates in Table 4.3

one in order to avoid error propagation. The results obtained for the configuration of receivers in Table 4.1 are shown in fig.4.13 which represents the absolute localization error in the time domain $|\widehat{p_u}(t) - p_u(t)|$ for $u = x, y, z$ and $t = k \cdot \frac{\Delta t}{2}$ where k is the iteration number of the location algorithm and $\frac{\Delta t}{2} = 0.25$ s.

A significant increase of the absolute error occurs for times greater than $t = 54$ s. For times greater than 54 s, the method is unable to keep localizing the aircraft because of the similarity between the values of the relative Doppler stretches (see section 4.1.2.1). Therefore, the influence of the similarity of the relative Doppler stretches in the resolution of the equation system is reaffirmed, and thus the error for times greater than $t = 54$ s (fig.4.13) is not due to the method of resolution of the equation system.

Table 4.4 lists the maximum and mean errors obtained within $t \in [0; 54]$ s. The percentages represent the contribution of these errors to the errors of the localization method in Table 4.2 for the straight flight path. The percentages show that the implemented genetic algorithm is responsible for about 25% of the errors in Table 4.2 of the location method described in this thesis. However, the mean error in the x-coordinate is smaller than the maximum displacement of the aircraft on the x-direction during 0.25 s which corresponds to 37.3 m in case of the straight trajectory.

TABLE 4.4: Evaluation of maximum and mean error in estimated aircraft position for each spatial coordinate x, y, z for the interval $t \in [0; 54]$ s.

u	max(Err_u) [m]	Percentage	$\widehat{Err}_u$ [m]	Percentage
x	52.19	21.04 %	27.3	51,37 %
y	5.46	7.0 %	1.09	5.7 %
z	10.6	7.28 %	4.0	9.2 %

4.1.2.3 Accuracy of the 1D ambiguity function

This section evaluates the accuracy of the method described in section 3.1.3 that is used to calculate the relative Doppler stretch values $\widehat{\delta f_{1n}}$ for receivers $n \in \{2, ..., 7\}$. The accuracy of the relative Doppler stretch calculations has a direct influence on the accuracy of the estimates of aircraft position, as shown in eq.(3.26). To focus only on the accuracy of the ambiguity function, we require the previous synchronization process (section 3.1.1) to be error free. To achieve a synchronization without error, the theoretical position of the aircraft - instead of the estimated one - has been used to

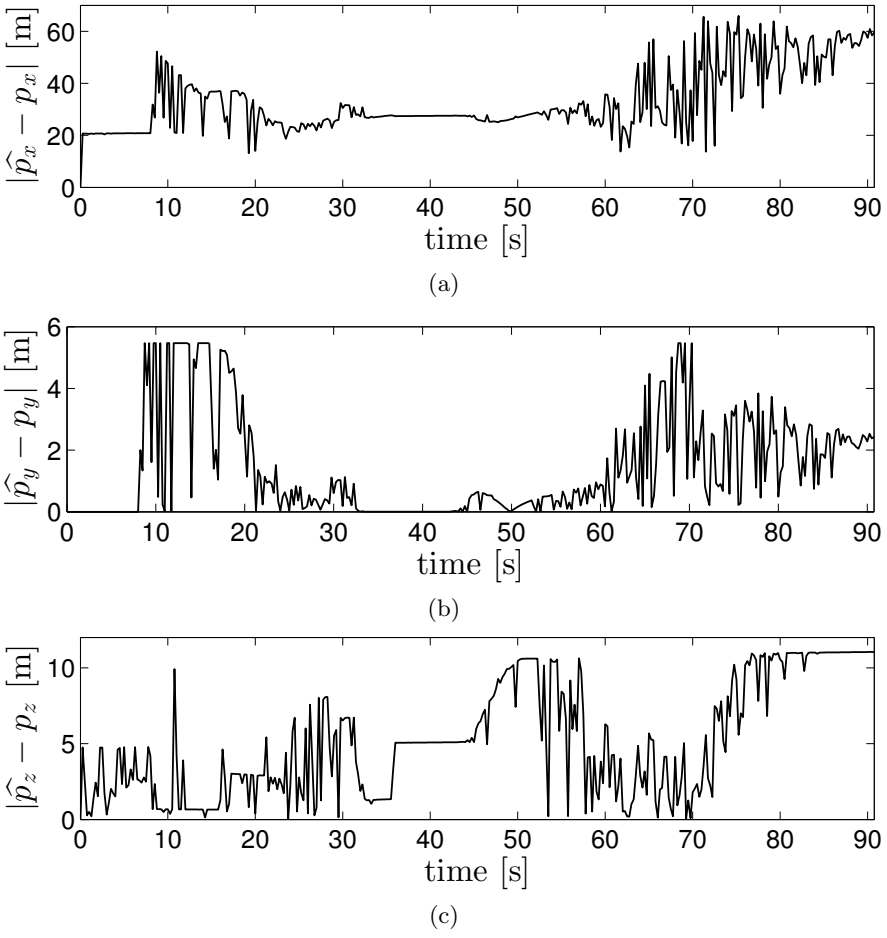

FIGURE 4.13: Absolute localization error for (a) the x- coordinate, (b) y-coordinate, and (c) z-coordinate, obtained by the acoustic method tested with the theoretical values of the Doppler stretches and theoretical restrictions of the genetic algorithm.

account for the sound propagation time from the aircraft position to the positions of the receivers.

Figure 4.14 shows the time evolution of the absolute error committed in the calculation of the relative Doppler stretches $\widehat{\delta f_{1n}}$ for all receivers $n \in \{2, ..., 7\}$ in Table 4.1. Since the theoretical aircraft position has been used to synchronize the signals at all receivers, the error obtained is totally caused by the 1D ambiguity function computation described in section 3.1.3. The maximum value of these errors $|\widehat{\delta f_{1n}} - \delta f_{1n}|$ for all receivers $n \in \{2, ..., 7\}$ is $8 \cdot 10^{-3}$ which is 15.9% of the maximum possible variation of δf_{1n} in an interval of $\dfrac{\Delta t}{2}$ s which is 0.05. The mean errors for all receivers are in the range of $3 \cdot 10^{-4}$ and $7 \cdot 10^{-4}$ which is less than the 1.4% of 0.05 (see section 3.2.2). It is convenient to note that relative Doppler stretches are calculated using a portion of the signals received by each receiver of duration Δt s. During this time interval and for

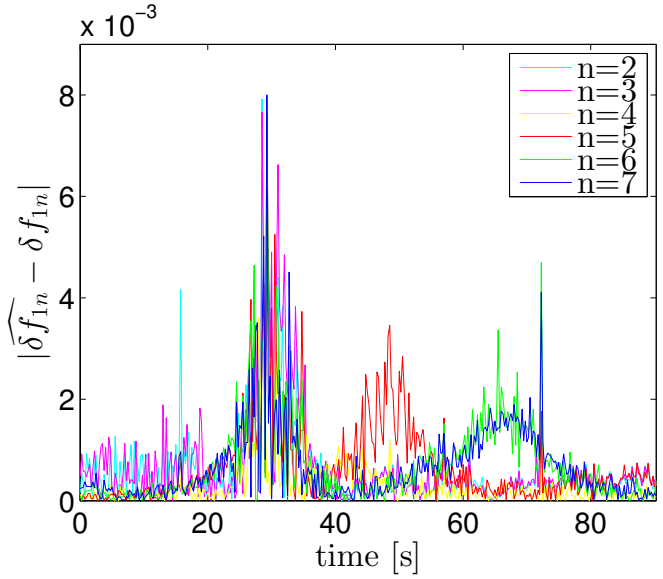

FIGURE 4.14: Time evolution of the absolute error of the relative Doppler stretches assuming the most-accurate in the synchronization process for all microphones $n \in \{2, ..., 7\}$ distributed according to Table 4.1

any $n \in \{2, ..., 7\}$, δf_{1n} is not strictly constant because of the continuous movement of the aircraft. Therefore, part of the error encountered is related to this inevitable fact and thus the accuracy of the method used to calculate the relative Doppler stretches is acceptable.

To show the influence of these errors on the final aircraft localization, fig.4.15 shows the absolute localization errors for each coordinate obtained from $\widehat{\delta f_{1n}}$. Table 4.5 gives the percentages of the maximum and mean localization errors obtained for this test with respect to the localization errors in Table 4.7.

TABLE 4.5: Evaluation of maximum and mean error in estimated aircraft position for each spatial coordinate x, y, z for time interval $[0; 54]$ s when the aircraft is up to 5.3 km far from the origin of coordinates.

u	$\max(Err_u)$ [m]	Percentage	$\widehat{Err_u}$ [m]	Percentage
x	50.8	20.0 %	8.4	15.8 %
y	5.46	7.0 %	2.9	15.17 %
z	10.6	7.28 %	3.0	6.9 %

The location errors are the result of both the method used to calculate the relative Doppler stretches and the genetic algorithm used to solve the equation system (3.18). However, the percentages observed in Table 4.5 are of the same order of magnitude as

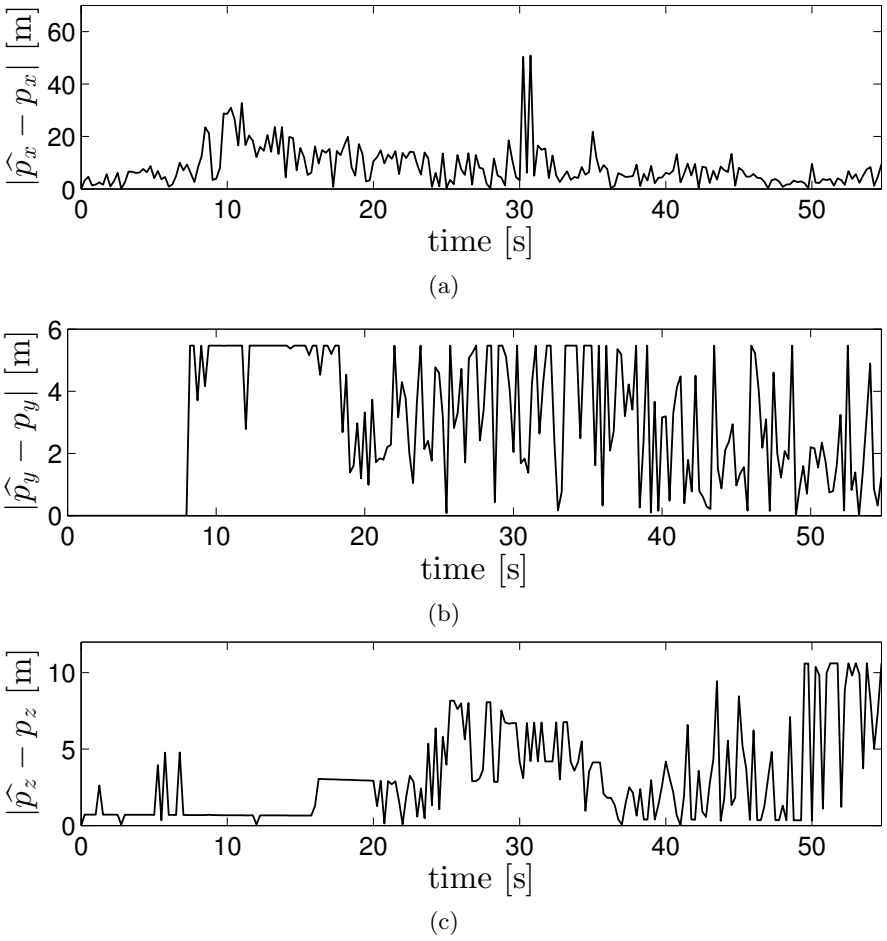

FIGURE 4.15: Absolute localization error for (a) the x- coordinate, (b) y-coordinate, and (c) z-coordinate, assuming no error in the synchronization process (section 3.1.1) for the Doppler stretch calculations and with theoretical restrictions of the genetic algorithm.

the ones given in Table 4.4 where the influence of the genetic algorithm in the location method was the only factor included. Therefore, the contribution of the ambiguity function used in the method to evaluate the values of δf_{1n}, in the total error of the location method is negligible.

4.1.2.4 Influence of the uncertainty in the estimate of initial position

The location method presented in this thesis requires the prior knowledge of the aircraft's effective liftoff position. In an actual implementation of the method for everyday use, the liftoff position and speed of the plane are rarely known with total accuracy. In this section, the possible maximum error in the estimate of the initial position and speed

is analyzed. The robustness of the method is shown when a biased initial position and speed are introduced.

The aircraft speed at the moment of liftoff is generally within 80 m/s (minimum value for the standard takeoff safety speed V_2) and 110 m/s. Therefore, the maximum possible speed error is the difference between these two extreme speeds, $110 - 80 = 30$ m/s. This error has been introduced in the take off direction given by the straight trajectory of fig.4.1, i.e., 29.24 m/s of error in the x-axis, and 6.7 m/s of error for height above ground in the z-axis.
The take off direction is along an extension of the runway centerline. Thus, the error in the initial position $\boldsymbol{p}^0$ will only affect the x-coordinate of the position (fig.4.1). The estimation of the initial position $\boldsymbol{p}^{*0}$ is related to the real position as follows

$$|\boldsymbol{p}^{*0} - \boldsymbol{p}^0| = \Delta x.$$

The maximum value of Δx that the method allows is determined by the synchronisation procedure. The relation between the propagation time $\Delta T_n^*(t^0)$ and the erroneous initial position $\boldsymbol{p}^{*0}$ is $\Delta T_n^*(t^0) = \dfrac{|\boldsymbol{r}_n - \boldsymbol{p}^{*0}|}{c}$ (section 3.1.4). The synchronization process selects a portion of the signal at each receiver starting at a time that does not correspond to the same emission time. The assumed time of starting is not crucial for the present method unless it differs from the correct one by as much as the length of the signal portion, which is Δt seconds. Hence, the following condition must hold:

$$|\Delta T_n(t^0) - \Delta T_n^*(t^0)| < \Delta t \qquad \forall n \in \{1, .., 7\} \tag{4.6}$$

which is equivalent to

$$||\boldsymbol{r}_n - \boldsymbol{p}^0| - |\boldsymbol{r}_n - \boldsymbol{p}^{*0}|| < \Delta t \cdot c \qquad \forall n \in \{1, .., 7\}. \tag{4.7}$$

Equation 4.7 depends on receiver position. However, it can be proven that $||\boldsymbol{r}_n - \boldsymbol{p}^0| - |\boldsymbol{r}_n - \boldsymbol{p}^{*0}||$ is maximum for a receiver aligned with the theoretical and erroneous initial position. In this case, $||\boldsymbol{r}_n - \boldsymbol{p}^0| - |\boldsymbol{r}_n - \boldsymbol{p}^{*0}|| = \Delta x$. As a consequence, the condition that must hold is

$$\Delta x < \Delta t \cdot c \tag{4.8}$$

Therefore, the initial position uncertainty of the aircraft must be less than $\Delta t \cdot c$. In the simulations presented here $\Delta t = 0.5$ seconds and $c = 340$ m/s so that the error

introduced in the x-coordinate of the aircraft initial position must be less than $\Delta t \cdot c = 170$ m.

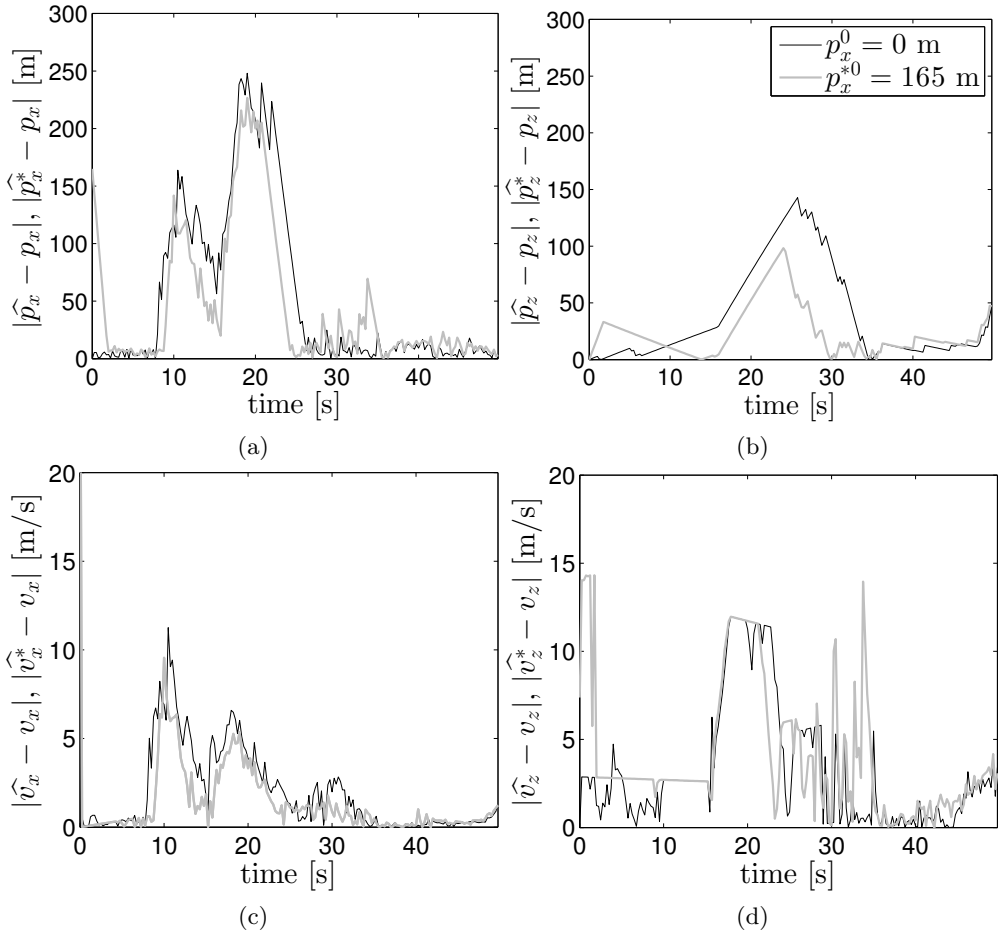

FIGURE 4.16: Absolute localization error of the method initialized with both an erroneous initial position (165 m of error) and the theoretical initial position p_x^0 for the straight trajectory of fig.4.5: a) refers to the x-coordinate of aircraft position, b) the z-coordinate of aircraft position, c) the x-component of aircraft speed, and d) the z-component of aircraft speed.

To analyze the performance of the method for $\Delta x < 170$ m, fig.4.16 represents the absolute localization error obtained by using the 165 m erroneous initial position and the maximum erroneous speed ($|\widehat{p_r^*} - p_r|$ and $|\widehat{v_r^*} - v_r|$), and the ones using the theoretical initial position and speed ($|\widehat{p_r} - p_r|$ and $|\widehat{v_r} - v_r|$). It can be seen that the errors for the simulation using the erroneous initial position decrease after 2 s for both spatial coordinates and both speed components. Afterwards, the error tends to be of the same order of magnitude as the one from the simulation using the theoretical initial position. In conclusion, it seems that the uncertainty in the location and airspeed at the initial position only influences the first location of the aircraft and does not affect the robustness

of the whole localization method, as long as the error in the initial position satisfies the criterion in eq.(4.8).

4.2 Omnidirectional source in a homogeneous medium

Section 4.1 has considered a simple sound propagation model. The present section describes a more complete model considering the atmospheric attenuation that influences the propagation of aircraft noise. The atmospheric attenuation modifies differently the frequency spectrum received by each receiver and could diminish the accuracy of the acoustic localization method. The performance of the method considering a homogeneous but non lossless propagation medium is assessed in this section. Moreover, the results and discussions in section 4.1.2 suggest that the accuracy of the method could be increased by not using a fixed reference microphone. At that aim, two different alternatives are explored in this section. Also, the influence of a possible uncertainty on the microphones synchronization is discussed here. Section 4.2.1 describes the method implementation and section 4.2.2 presents the results obtained from the computer simulation.

4.2.1 Description of the computer simulation

4.2.1.1 Setup

The aircraft trajectory used in the present simulation is the straight trajectory in fig.4.1. Figure 4.17 depicts the time evolution of the aircraft acceleration module and the acceleration elevation angle. Although the flight path is contained in a known plane ($y = 0$) and the location problem could be treated as a two-dimensional problem, the simulation of the method has been done as a three-dimensional localization. This means that no restrictions have been imposed concerning neither the y-coordinate of the aircraft nor the y-component of velocity.

The seven microphones used are distributed as shown in fig.4.18. The initial position of the aircraft is considered to be the start of takeoff at the time of liftoff as it is in the previous sections. This position is the origin of coordinates for the receivers coordinates listed in Table 4.6 and for further aircraft positions.

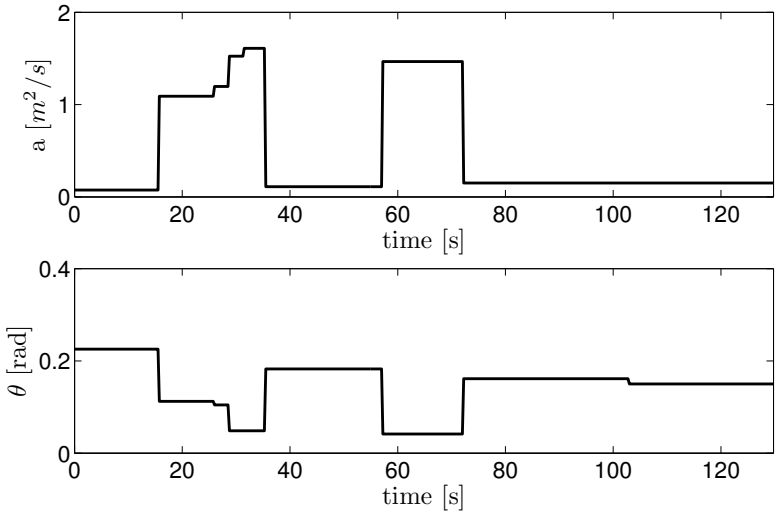

FIGURE 4.17: The modulus of the aircraft acceleration vector and the elevation angle of the aircraft acceleration vector as a function of time (clock-wise relative to the z-axis in fig.4.18) are represented on the top and the bottom of the figure respectively as a function of time after liftoff

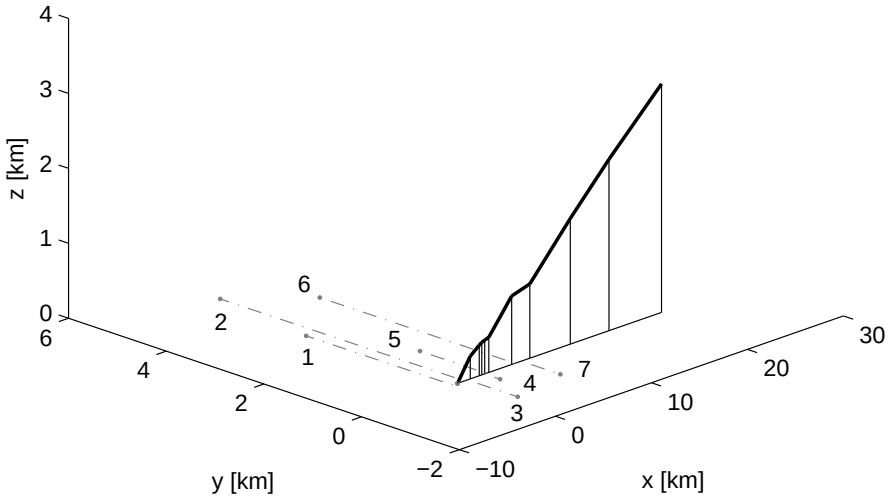

FIGURE 4.18: Flight path geometry and receiver locations. The aircraft trajectory is parallel to the x-axis from liftoff at $x = 0$, $y = 0$, $z = 0$. The numbered dots designate the positions of the seven receivers.

The microphone distribution is similar to the third distribution tested in section 4.1.2.1. Microphones have been enumerated in ascendent order of their x-coordinates, the direction in which the aircraft is moving.

TABLE 4.6: Position of the receivers $n \in \{1, .., 7\}$ with respect to the origin of coordinates

n	1	2	3	4	5	6	7
r_{nx} [m]	-500	720	1040	2800	3000	6000	6640
r_{ny} [m]	3000	5000	-1028	-320	1360	4000	-800

4.2.1.2 Aircraft sound-propagation model

Equation (4.2) shows the relationship between the sound pressure signal at a receiver n and the strength of the source in the case of considering only the geometrical spreading. However, this propagation model is simple when applying the acoustic method for aircraft localization. The atmospheric absorption influences the aircraft sound propagation due to the large distances between the aircraft and receivers and needs to be considered.

Transforming eq.(4.2) into the frequency domain and introducing the atmospheric attenuation for sound propagation outdoors as given in ISO 9613-1:1996 [36], the amplitude of the sound pressure spectrum of receiver n is expressed by:

$$|Y_n(f')| = \left[\frac{c}{c - |\boldsymbol{v}| \cdot \cos(\alpha_n)}\right] \cdot \frac{e^{-\alpha(f)\cdot \boldsymbol{q}_n}}{4\pi|\boldsymbol{q}_n|} \cdot |Q(f)|. \tag{4.9}$$

The amplitude scale factor in eq.(3.2) corresponds here to:

$$\rho_n = \left[\frac{c}{c - |\boldsymbol{v}| \cdot \cos(\alpha_n)}\right] \cdot \frac{e^{-\alpha(f)\cdot \boldsymbol{q}_n}}{4\pi|\boldsymbol{q}_n|} \tag{4.10}$$

where $\alpha(f)$ is the atmospheric absorption coefficient whose calculation is described in detail in ISO 9613-1:1996 [36] and depends on the emitted frequency, temperature, air pressure and relative humidity. Its simplified expression is as follows:

$$\begin{aligned}\alpha(f) = 1.84 \times 10^{-11} \left(\frac{T}{T_0}\right)^{1/2} \frac{F^2 p_s}{p_{s^0}} \\ +0.01278 \frac{e^{-2239.1/T}}{F_{r,O} + F^2/F_{r,O}} \left(\frac{T}{T_0}\right)^{-5/2} \frac{F^2 p_s}{p_{s^0}} \\ +0.1068 \frac{e^{-3352/T}}{F_{r,N} + F^2/F_{r,N}} \left(\frac{T}{T_0}\right)^{-5/2} \frac{F^2 p_s}{p_{s^0}}\end{aligned} \tag{4.11}$$

where p_{s^0} [atm] and the T_0 [K] are the reference atmospheric pressure and temperature (1atm and 293.15 K respectively), p_s [kPa] and T [K] are the atmospheric pressure and

temperature at the measurement time (in this simulation they are set to be 102.42 kPa and 288.15 K (15°C)), the term $F = f/p_s$ where f [Hz] is the frequency of the emitted sound, $F_{r,O}$ and $F_{r,N}$ are the relaxation frequencies of Oxygen molecules and Nitrogen molecules in the atmosphere and the governing expressions are given in ref.[37].
The frequency and distance dependence of the atmospheric attenuation term in eq.(4.9) shows the significant sound pressure level amplitude attenuation at higher frequencies and larger distances.

The sound pressure at each receiver n is reconstructed by eq.(4.9) using as inputs the aircraft strength frequency spectrum of fig.4.3, the aircraft flight path of fig.4.18, and the aircraft velocity calculated from fig.4.17.

4.2.1.3 Implementation

The implementation for this computer simulation considering a homogeneous but non lossless medium corresponds to the same description in section 4.1.1.3 regarding the initialization, the parameters to be selected, the calculation of relative Doppler stretches and the calculation of the aircraft position. The reason is that the selection of all variables required for the localization method to be implemented does not depend on the sound propagation model considered.

4.2.2 Results

4.2.2.1 Influence of the atmospheric attenuation

One of the particulars of the acoustic localization method applied to aircrafts is the influence of the atmospheric attenuation on the aircraft sound propagation. The experimental validation of the method presented in ref.[27] locates a sound source moving at constant speed along a linear path. The microphones used for this test were located close to the sound source trajectory and the effect of the atmospheric attenuation on the sound propagation was insignificant. The application presented in this thesis is a three-dimensional localization and contemplates larger distances between receivers and the moving sound source. Because of this spatial extension, the absorption of the propagation medium influences the transmitted sound and has been included on the sound propagation model used in the present simulation test (section 4.2.1.2). Note that the atmospheric attenuation alters the main component of the method, the receivers'

frequency spectra $X_n(f)$. Equation (4.11) shows the frequency dependence of the attenuation coefficient, $\alpha(f)$, and its proportionality to the square of the emitted sound frequency. Hence, the original wideband frequency spectrum of the aircraft is distinctly modified at each frequency component. The higher the frequency, the stronger the attenuation. Furthermore, the effect of the atmospheric attenuation varies with respect to the distance from the sound source. Since all receivers used for this new acoustic localization method are at an arbitrary distance from the aircraft, their frequency spectra are affected differently by the atmospheric absorption.

The variations in the received spectra, in addition to the different scale factors in the frequency domain due to the Doppler effect, affect the calculation of the 1D ambiguity function (see eq.(3.21)) which measures the similarity between two relatively compressed spectra. The accuracy of the results obtained from this calculation are critical since they are used to obtain the values of the relative Doppler stretches, which in turn are the input arguments of the system of equations determining the aircraft position.

To appreciate the influence of the atmospheric attenuation on the localization method, figs.4.19 and 4.20 show the estimated aircraft trajectory obtained considering a lossless and a homogeneous but non lossless sound propagation medium respectively.

The results are presented for each spatial coordinate, x, y and z. In both cases the method clearly ceases to track the aircraft at $t = 40$ s when the aircraft is 3700 m away from the initial takeoff position in the horizontal plane and at 555 m of altitude. Up to that point, no significant differences can be seen in the localizations. Table 4.7 lists the maximum and mean errors obtained during the localisation time interval $t \in [0; 40]$ for both tests and for each spatial coordinate. The mean error has been already defined in eq.(4.4).

TABLE 4.7: Evaluation of the maximum and mean error reached by each spatial coordinate x, y, z for the time interval $[0; 40]$ s

	u	$\max(Err_u)$ [m]	$\widehat{Err}_u$ [m]
Lossless medium	x	44.88	10.35
	y	20.20	5.43
	z	54.53	20.08
Homogeneous medium	x	113.6	24.82
	y	47.39	10.37
	z	60.13	30.36

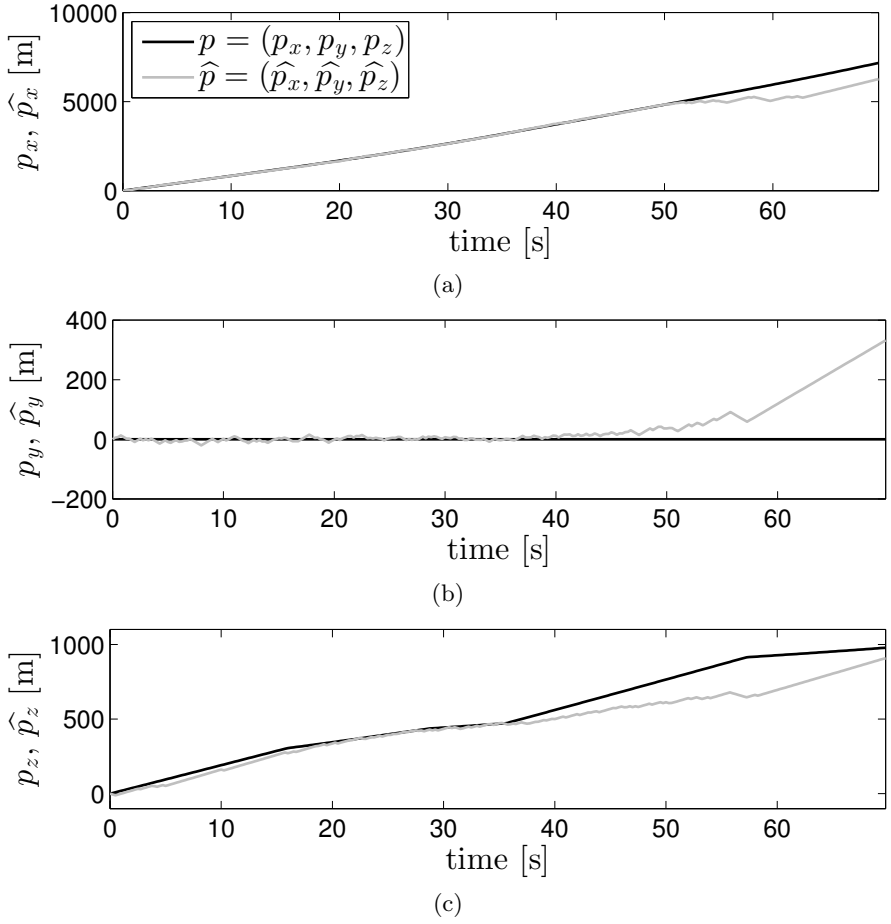

FIGURE 4.19: Theoretical (p) and estimated ($\widehat{p}$) aircraft position under the lossless medium consideration: (a), (b) and (c) represent the projections of the flight path on the x-axis, y-axis, and z-axis respectively.

The errors obtained considering a lossless medium are lower than those for the homogeneous medium. Importantly, however, the mean errors for both cases are of the same order of magnitude as the dimensions of a standard commercial aircraft and do not exceed the dimensions of the Airbus 318, one of the smaller civil aircraft commonly used.

4.2.2.2 Alternative to the microphone of reference

The results in section 4.2.2.1 have been obtained by choosing microphone number 1 of Table 4.6 as the reference microphone to compute the relative Doppler stretches. To evaluate the influence of this choice on the location method, each microphone of Table 4.6 has been tested as a reference microphone. Figure 4.21 shows the different results obtained for each of them. For microphones 4 and 5, the localization fails at $t = 25$ s

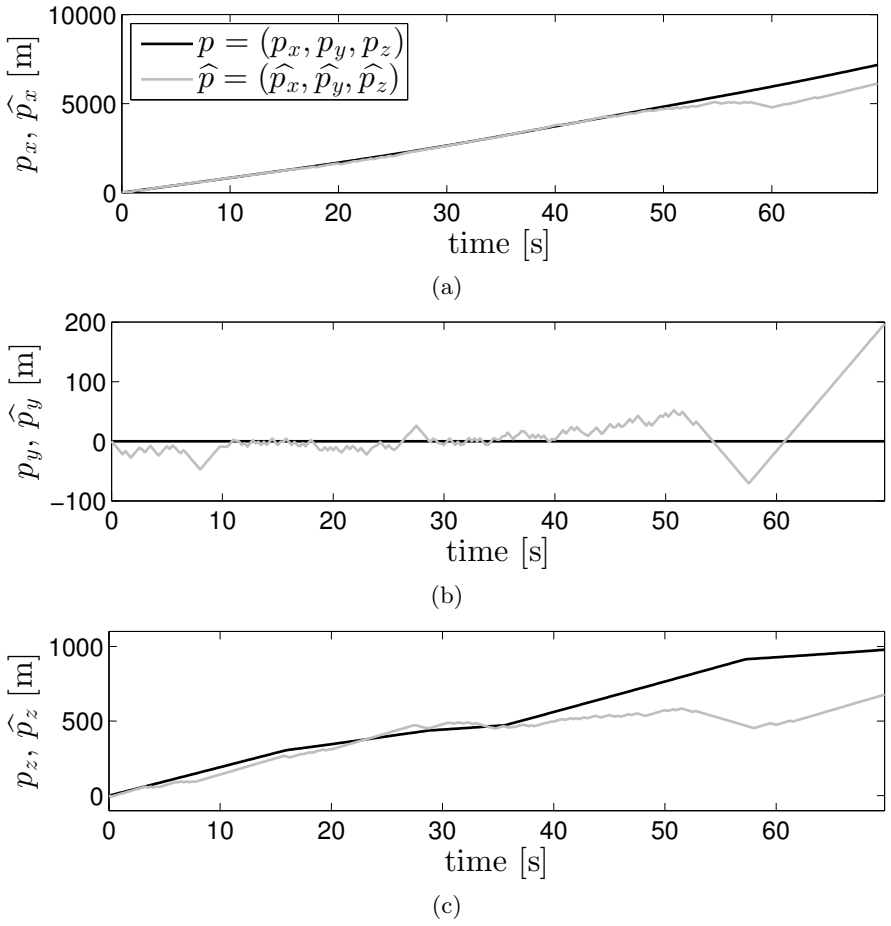

FIGURE 4.20: Theoretical (p) and estimated ($\widehat{p}$) aircraft position under the homogeneous medium consideration: (a), (b) and (c) represent the projections of the flight path on the x-axis, y-axis, and z-axis respectively.

and $t = 15$ s respectively, and for the rest of the microphones, at $t = 40$ s. Therefore, not all receivers are suitable as a reference microphone and some criterion must be found for an optimal selection.

In section 4.1.2.1, it is seen that when the six relative Doppler stretches have similar values, the acoustic method does not detect any difference between them and fails in the localization process. Therefore, a good test of the fitness of the reference microphone selection is the value of relative Doppler stretches that result. However, relative Doppler stretches vary as a function of the aircraft motion with respect to the microphones distribution (see eq.(3.18)) and thus, their values can not be predicted without prior knowledge of the aircraft trajectory.

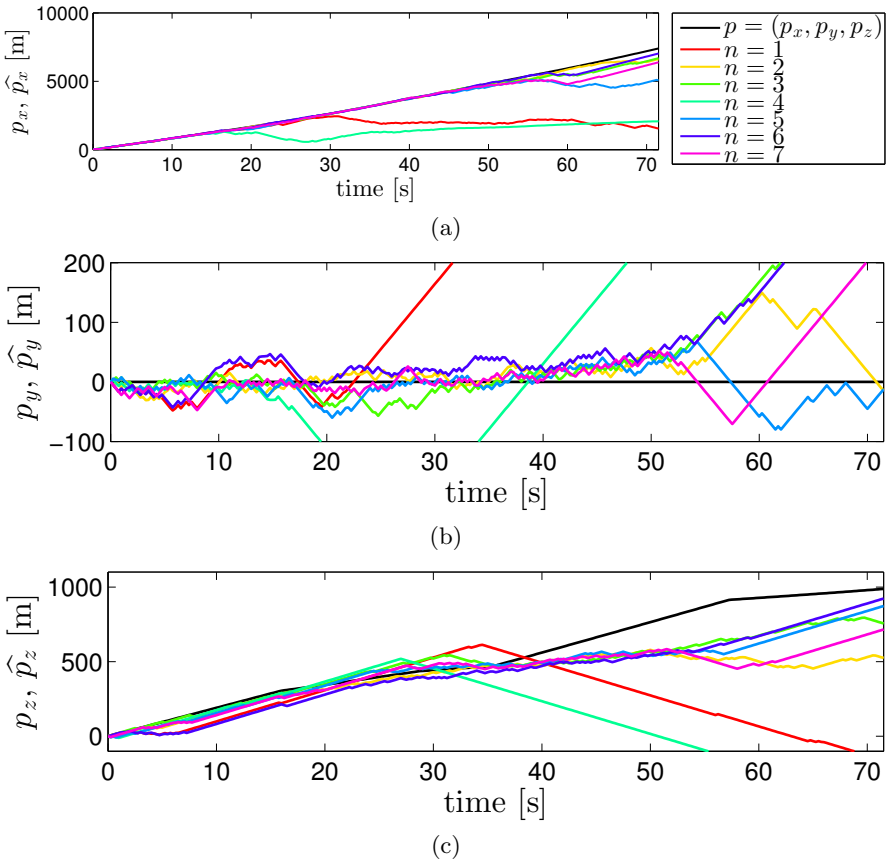

FIGURE 4.21: Localization results using microphone number n as the reference microphone: (a), (b) and (c) represent the projections of the flight path on the x-axis, y-axis, and z-axis respectively.

To avoid this trajectory dependence, it is proposed here to remove the concept of microphone of reference. The use of seven receivers allows the parallel calculation of 42 relative Doppler stretches. As the similitude between the relative Doppler stretches is a drawback for the location algorithm, a good strategy can be to select a set of six values (among the 42) as different as possible. With that aim, several techniques can be applied to evaluate the fitness of a set of values. The standard deviation of the six values or the standard deviation of the differences between the consecutive stretches of the set can be used as a fitness measure. The greater the deviation, the better the set of relative Doppler stretches.

However, the technique suggested here does not evaluate all possible sets of six values of relative Doppler stretches, but deals directly with the 42 values to determine the more suitable set. The selection technique consists of the following two steps:

1. Selection of the maximum and minimum values among all 42 relative Doppler stretches not the inverse of one another (note that if a relative Doppler stretch

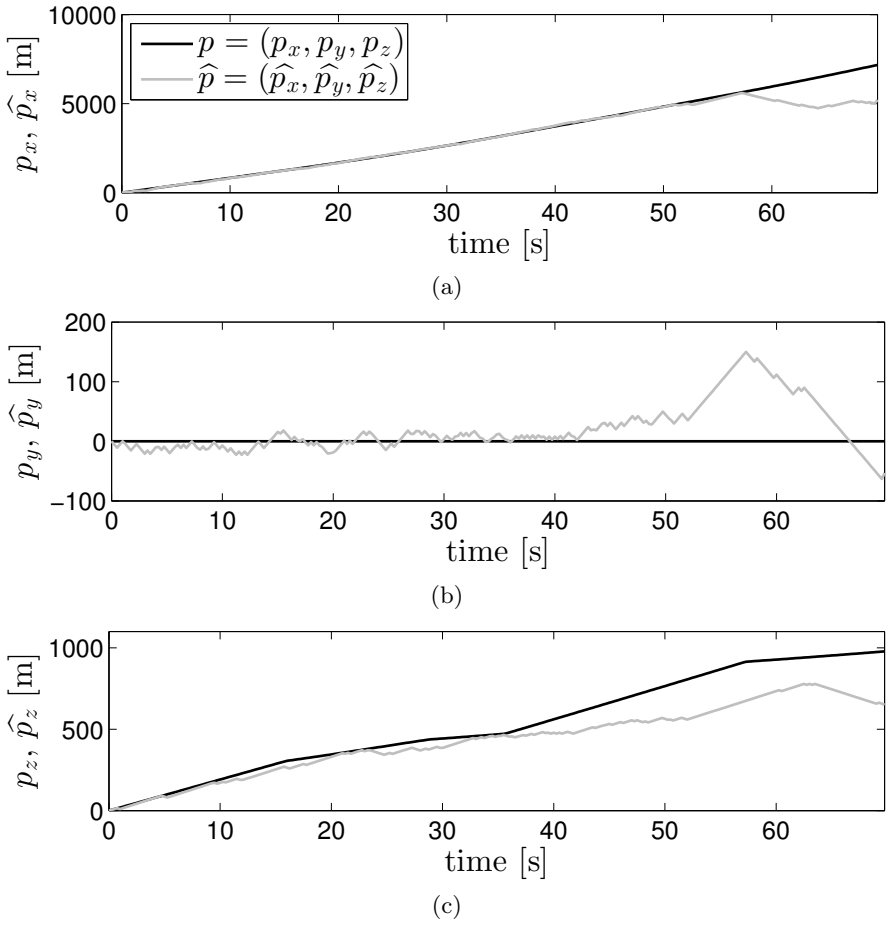

FIGURE 4.22: Localization obtained for each spatial coordinate x, y, z by using the set of the most different values of six Doppler stretches

δf_{mn} is the maximum, the minimum will be its inverse δf_{nm}; when a Doppler stretch is selected, its inverse must be discarded from the possible values further selected).

2. Division of the range defined by the minimum and maximum stretches by four equidistant separations and select the relative Doppler stretches closest to these divisions.

The set of six values obtained is the set containing the most equidistant relative Doppler stretches, and therefore, the set of stretches most different among the 42 values. Applying this criterion at every iteration of the location method, the estimated aircraft trajectory is represented in fig.4.22 and the maximum and mean errors for each spatial coordinate within the time interval $t \in [0; 40]$ are listed in Table 4.8.

TABLE 4.8: Evaluation of the maximum and mean error of the localization results for each spatial coordinate x, y, z for the time interval $[0; 40]$ s using the set of the most different values of six Doppler stretches

u	$\max(Err_u)$ [m]	$\widehat{Err}_u$ [m]
x	80.45	19.46
y	22.70	9.17
z	82.73	27.28

The errors obtained here are lower than those of Table 4.7 where microphone 1 was used as the reference microphone (assuming a homogeneous medium) although they are of the same order of magnitude.

The use of only six values of relative Doppler stretches leads to a system of only six equations (3.18) describing the aircraft position and speed. If one of the six calculated Doppler stretches is erroneous, then one of the six equations is not well-stated and does not describe a coherent aircraft localization. To minimize the influence of a possible error on the calculation of a Doppler stretch, all 42 values of Doppler stretches have been used as inputs to the equation system using the same microphone distribution of Table 4.6. Figure 4.23 shows the location results obtained by using all 42 values of Doppler stretches versus the expected theoretical trajectory. To appreciate the errors committed in this aircraft localization, Table 4.9 lists the maximum and mean errors obtained for each spatial coordinate.

TABLE 4.9: Evaluation of the maximum and mean error of the localization results for each spatial coordinate x, y, z for the time interval $[0; 40]$ s using the 42 values of Doppler stretches

u	$\max(Err_u)$ [m]	$\widehat{Err}_u$ [m]
x	126.5	18.42
y	36.13	8.62
z	48.19	20.01

These errors are similar to the errors obtained by the selection of the six more convenient values of Doppler stretches (Table 4.8). The modulus of the mean location error, $|\widehat{Err}_p| = \sqrt{\widehat{Err}_x^2 + \widehat{Err}_y^2 + \widehat{Err}_z^2}$, is 28.53 m in this test (Table 4.9) and 34.74 m in the case of the most different six Doppler stretches selection (Table 4.8).
Therefore, the use of a suitable reference microphone seems to be equivalent in terms

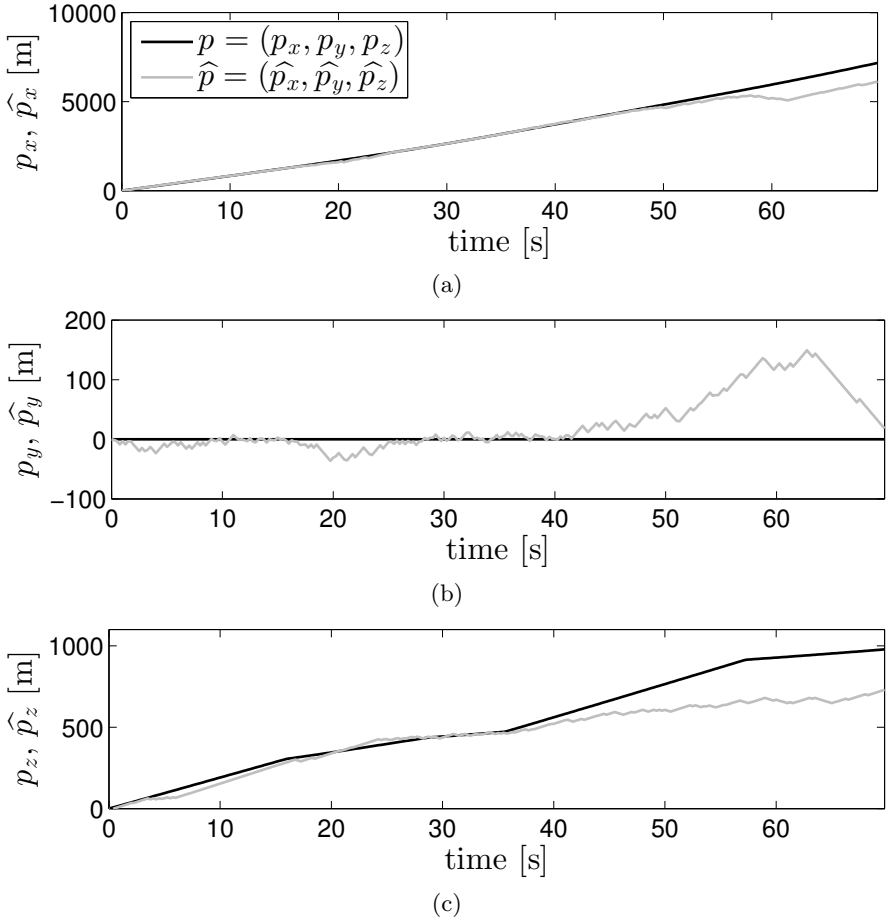

FIGURE 4.23: Localization obtained for each spatial coordinate x, y, z by using all 42 values of Doppler stretch

of the location results to both the selection of the more convenient values of Doppler stretches and to the use of all calculated Doppler stretches.

Both alternatives to the use of a microphone of reference are still dependent on the aircraft flight path since Doppler stretches do. However, both of them increase the location accuracy, and in particular the one using all 42 Doppler stretches decreases the influence of a possible incoherent equation due to an erroneous value of Doppler stretch.

4.2.2.3 Influence of the microphones synchronization error

The real implementation of the acoustic localization method will involve synchronization errors between the whole sensor network. To simulate this sensors synchronization inaccuracy, a random value between $(-s\% \cdot \Delta t)$ and $(s\% \cdot \Delta t)$ where s is previously fixed is added to each microphone. To appreciate only the influence of the microphone

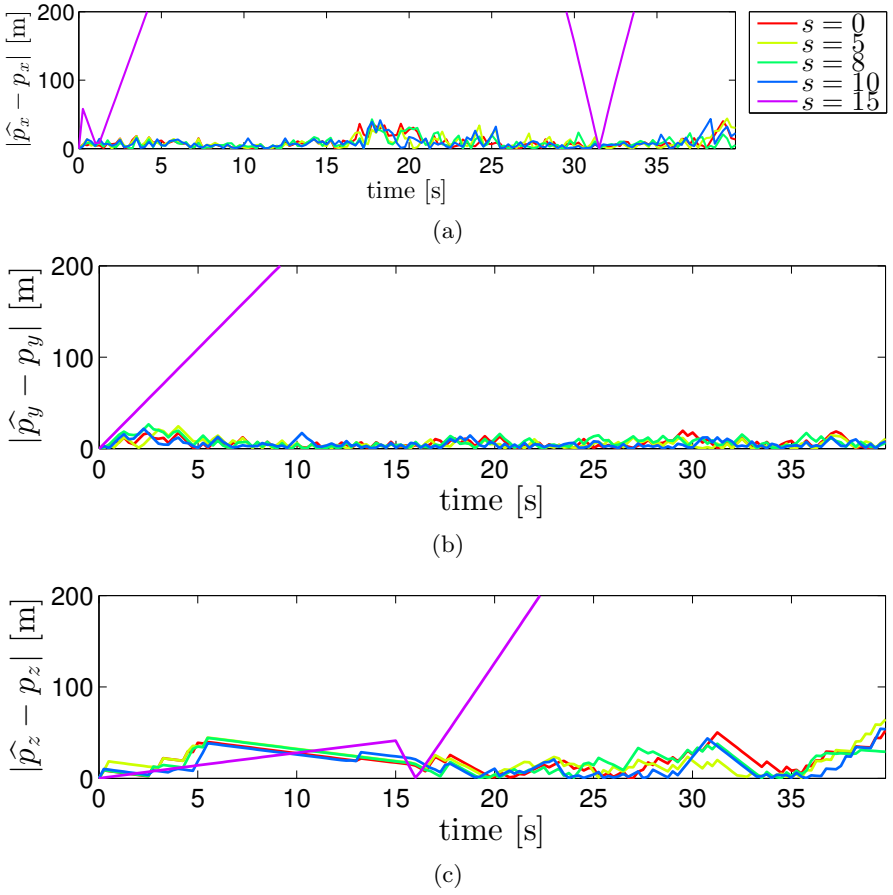

FIGURE 4.24: Absolute localization error during the time interval $t \in [0; 40]$ s for the three spatial coordinates (a) x, (b) y and (c) z and for each fixed percent value s of Δt used to simulate the inaccuracy of the microphones synchronization.

synchronization inaccuracy on the localization method, the compensation of the retardation effect on the received signals (section 3.1.1) is done using the theoretical value $\boldsymbol{p}(t^o)$ instead of the estimated value $\widehat{\boldsymbol{p}}(t^o)$.
Figure 4.24 shows the absolute localization error, $|\widehat{p}_u - p_u|$ for $u = x, y, z$, obtained for each tested value $s \in \{5, 8, 10, 15\}$. The case $s = 0$ corresponds to the ideal case without error on the microphone synchronization process.

The absolute localization errors are similar for the cases of error synchronization up to 10% of Δt. For the three cases $s = 5, 8$ and 10, the modulus of the mean location error $|\widehat{Err_p}|$ (eq.4.4) during the time interval $t \in [0; 40]$ s is in the range of $[9.84; 11.56]$ m which is lower than the dimensions of an standard commercial aircraft. The robustness of the localization method is therefore not altered for synchronization errors up to 10% of Δt. Actually, the synchronization accuracy ensured nowadays by providers of sensors

networks is up to $2 \cdot 10^{-6}$ s which corresponds to $4 * 10^{-4}$ % of the value of Δt used in the simulations included in this thesis.

Chapter 5

Experimental validation

In order to validate experimentally the acoustic localization method described in chapter 3, an experimental test has been carried out in an airfield with a radio control airplane. Although the method has been developed for the localization of commercial aircraft, a full scale test in the surroundings of an airport is rather complicated to manage. It involves large distances between the acoustic sensors, the need to access to the at least seven measurement points, and a considerable amount and high budget resources. The experimental validation presented in this work has been carried out as a previous step to the further realization of a more complex test (in terms of management) in the surroundings of an airport where light aircraft operates.

The goal of the present test is to compare the airplane trajectory estimated by the acoustic method and the trajectory given by a Global Positioning System mounted on the airplane. This experimental validation of the acoustic method is a challenging test compared to a full scale validation. The radio control airplane experiences sudden significant variations of altitude and speed that influences the Doppler effect appreciated by the microphones. Moreover, the distances between microphones are small and thus, the influence of Doppler effect for each microphone tends to be similar when the airplane moves away from them. Note that both the behavior of the altitude and speed and the small distances between the acoustic sensors will not occur in an experimental test with a commercial aircraft. Then, the experiment has been definitely a challenge to validate the acoustic localization method.

The present chapter is organized as follows: section 5.1 describes the experimental setup, section 5.2 analyzes the test prior to the assessment of the localization results and section 5.3 presents and discusses the results obtained.

5.1 Setup

5.1.1 Airfield

The experimental test has been carried out in the airfield of the Aeronautic Club Egara in Terrassa (Spain). It is placed at the outskirts of the city in an area where the background noise is low. It is not surrounded by any building that could introduce reflections of the sound emitted by the radio control airplane. The airfield is placed in more or less rectangular flat area of 120 m long by 45 m wide of sandy soil. The runaway is made of artificial grass and it is 72 meters long by 15 meters wide. Figure 5.1 is a draft showing a top view of the airfield.

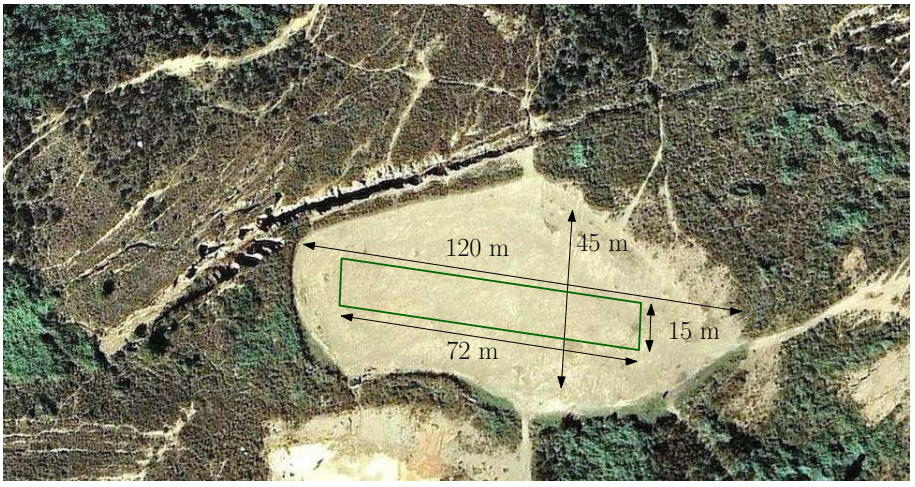

FIGURE 5.1: Airfield of the Aeronautic Club Egara, Terrassa

5.1.2 Radio control airplane

The sound source used consists on a radio control airplane with a 4-stroke engine (fig. 5.2a). Figure 5.2b shows the frequency spectrum of the airplane. This spectrum has been recorded at 2 meters from the airplane which was hold static at some meters over the ground while the engine was running. It can be seen from Figure 5.2b that is a tonal spectrum including multiples of the engine speed. Therefore, the frequency spectrum is highly dependent on the engine speed. The maximum speed of such an airplane is about 120 km/h (33 m/s).

a) Radio control airplane

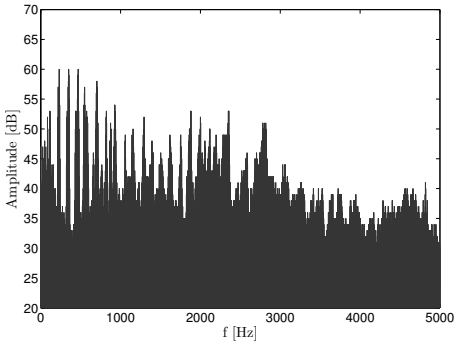

b) Frequency spectrum of the radio control airplane

FIGURE 5.2

5.1.3 Equipment for data acquisition

Airplane positioning data

To evaluate the performance of the acoustic localization method, the estimated trajectory needs to be compared with the real trajectory of the radio control airplane. In an attempt to obtain the exact trajectory of the plane a GPS system and a Multi altimeter from RC-electronics were mounted on the radio control airplane. Both devices are lightweight, the GPS is only 9 grams and the Multi altimeter is 6 grams so the airplane radio control is not altered. The GPS module calculates its position on Earth and provides longitude, latitude, altitude and ground speed over time. These data are sent to the Multi altimeter module that records them for later computer review. The position of the airplane is provided by the GPS system with a frequency rate of 5 Hz, this is every 0.2 seconds. The accuracy of these modules is of 3 meters meaning that the real position of the airplane can be within a sphere of radius 3 meters centered around the provided position.

Microphone positioning data

The eTrex Venture GPS from Garmin has been used in this experimental test to obtain the position of the seven microphone locations. The coordinates of the seven microphones positions have been used in the Universal Transversa Mercator (UTM) system of coordinates. These coordinates system is a Cartesian system with horizontal axis (x-axis) pointing to the east in the east-west direction and vertical axis (y-axis) pointing to the north in the north-south direction. Therefore, it is a convenient system to deal with in the concerned experimental validation.

The eTrex Venture GPS has an accuracy of 3 meters as the GPS used on the radio control airplane.

Acoustic data

The acoustic data during the experimental test have been recorded by the multi-channel system PIMENTO from LMS. Despite the distances of the test, all microphones have been connected by cable to the channels of the acquisition system.

The seven microphones used are G.R.A.S Type 40 AE and the pre-amplifiers G.R.A.S Type 26 CA. All of them were calibrated previously with a CESVA CB-5 calibrator Class 1L.

Concerning the placement of the microphones, true flush surface microphones have been used instead of microphones mounted on a tripod. The reason is to avoid the interference effect between the incident direct wave and the one reflected by the soil. To that aim, seven circular ground plates [38] of 1 meter of diameter have been built up for the test and each microphone has been located in the center of the circumference with half foam windscreen as shown in fig.5.3.

FIGURE 5.3: True flush surface microphones used for the experimental validation of the acoustic method for aicraft localization.

Synchronization of both positioning and acoustic data

In order to synchronize both the GPS mounted on the radio control airplane and PIMENTO acquiring the acoustical data from the seven microphones, both devices started recording at the time instant when the airplane starts moving along the runaway. Thus, the temporal origin t=0 s of both data coincides. The location of the airplane is given by the GPS every 0.2 s which means that the aircraft position $\boldsymbol{p}(t)$ is known each $t = k \cdot 0.2$ s for $k \in \mathbb{N}$. Therefore, the initial position $\boldsymbol{p}(t^0)$ required by the acoustic location method can be chosen from any recorded position $\boldsymbol{p}(k \cdot 0.2)$. Then, all seven sound signals can be considered from $k \cdot 0.2$ s (setting

that time as their time origin $t^0 = 0s$) and thus, the acoustic method is able to proceed with its first process of synchronization (section 3.1.1).

5.1.4 Microphone distribution

In section 4.1.2.1, it has been seen that the higher the difference between all relative Doppler stretches, the better the accuracy on the localization results. Then, an appropriate microphone distribution is the one producing the more different values of relative Doppler stretches along the airplane trajectory, or what is equivalent, the more different values of angles α_n between the airplane velocity $\boldsymbol{v}$ and the pathlength vector $\boldsymbol{q}_n$ pointing from the airplane to the receiver n (see fig.4.4). Both relative Doppler stretches and angles are dependent on the airplane trajectory. The expected aircraft path for this test is a constant height and speed trajectory along the runaway axes, but the real path will actually depend on the wind influence and the skill of the pilot. Since there is no prior knowledge of the exact real path, the expected trajectory is considered to distribute the microphones. Apart from this observation related to the Doppler stretch values, section 4.1.2.1 remarks that when the distance between the microphones is much smaller than the distance between the microphones and the source, the value of all the relative Doppler stretches tends to 1 (or equivalently $\alpha_n \approx 180\,\text{deg}$ for all $n \in \{1, .., 7\}$) and the localization fails. Therefore, the criteria used for the microphone distribution is that of covering the whole length of the runaway so the time interval while the source is trackable is longer (at least as long as the airfield length). Figure 5.4 shows the final microphone distribution together with the expected airplane trajectory of constant altitude of 33 m and constant speed of 26 m/s (data suggested by the pilot).

According to the expected trajectory in fig.5.4, the value of the relative Doppler stretches δf_{mn} computed from eq.(3.18) for $m \neq n$, $m, n \in \{1, .., 7\}$ are shown in fig.5.5. It can be seen that δf_{mn} for all m and n are distinguishable for each time $t \in [0; 8]$ s. Thus, the chosen microphone distribution seems to be appropriate (in terms of relative Doppler stretches) for the acoustic method assuming the airplane flies along the expected trajectory in fig.5.4.

Table 5.1 lists the Universal Transversa Mercator (UTM) coordinates in Zone 31T of the seven microphones given by the eTrex Venture GPS from Garmin (see section 5.1.3) used for the tests. However, the large values of these coordinates in our case are unwieldy to work with. To reduce their range, the position of microphone 1 is set as the new

FIGURE 5.4: Microphone distribution together with the expected airplane trajectory

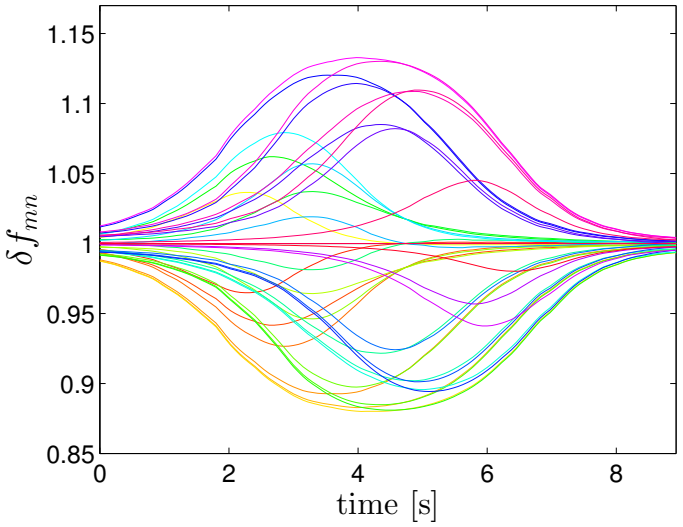

FIGURE 5.5: Time evolution of relative Doppler stretches along the expected trajectory of the radio control airplane

TABLE 5.1: UTM Coordinates for each microphone $n \in \{1, ..., 7\}$ distributed over the airfield.

n	1	2	3	4	5	6	7
r_{nx} (Easting) [m]	416407	416380	416384	416349	416334	416313	416303
r_{ny} (Northing) [m]	4603168	4603174	4603141	4603169	4603117	4603108	4603104

origin of coordinates without loss of generality. All coordinates presented from now on are relative to this new origin. Table 5.2 lists the reset coordinates and fig.5.6 shows the receivers distributed on the airfield together with the expected trajectory of the airplane.

TABLE 5.2: Coordinates of Table 5.1 for each microphone $n \in \{1, ..., 7\}$ with the new origin set to the position of microphone 1.

n	1	2	3	4	5	6	7
r_{nx} (Easting) [m]	0	-27	-23	-58	-73	-94	-104
r_{ny} (Northing) [m]	0	6	-27	1	-51	-60	-54

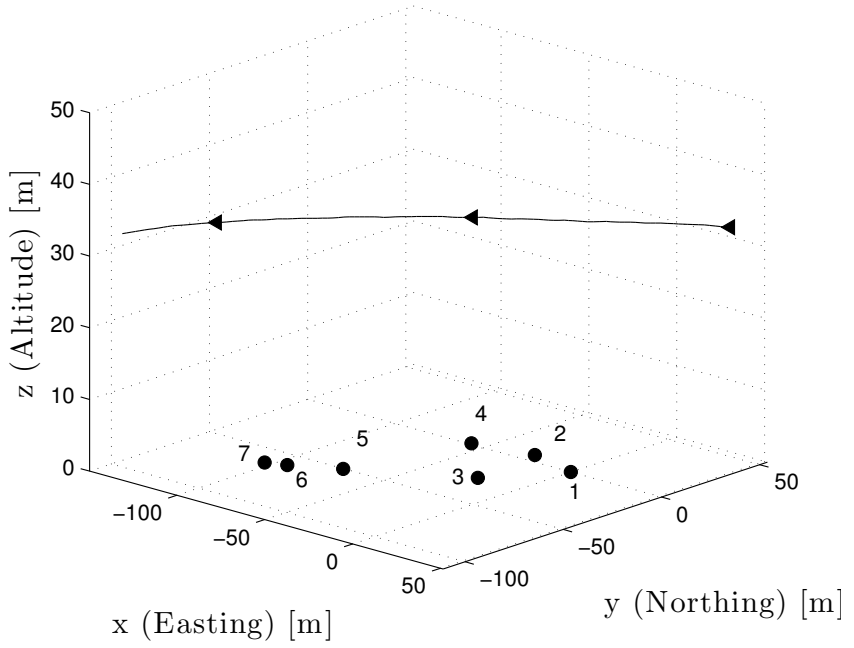

FIGURE 5.6: Microphone distribution together with the expected aircraft trajectory

5.1.5 Implementation

Initialization

To initialize the acoustic location method, an initial position of the airplane needs to be known. The coordinates of this initial position in fig.5.6 (with microphone 1 as the origin of coordinates) are $\boldsymbol{p}^0 = (41.4, 43.9, 35.1)$ m and the time corresponding to this position is set to $t^o = 0$ s. To appreciate how far is the airplane from the microphones at that time instant, Table 5.3 lists the distances from the airplane to each receiver n.

TABLE 5.3: Distances from the airplane being at the initial position $\boldsymbol{p}^0$ to each n-microphone location, $n \in \{1, ..., 7\}$.

n	1	2	3	4	5	6	7
Distance [m]	69.8	85.8	101.9	113.6	152.6	174.5	183.7

Parameters

The sample frequency rate f_m for all microphones has been of 5000Hz to avoid aliasing in the significant frequency content in fig.5.2b emitted by the radio control airplane which goes up to 2500Hz. The time interval Δt for this test according to the conditions in section 3.2.1 is set to 0.15 s. Then, the frequency resolution of the Fourier Transform of all receivers signal is 6.6 Hz which is an acceptable resolution taking into account the frequency spectrum emitted by the airplane (fig.5.2b). As a consequence of this choice, the acoustic method locates the radio control airplane every $\frac{\Delta t}{2} = 0.075$ s.

The Doppler stretch values used to estimate each airplane position are then calculated from the seven signal portions of $\Delta t = 0.15$ s. These stretch values can be associated to any time t within $[0; 0.15]$ s since Doppler stretches are not constant during Δt s due to the continuous airplane motion. Therefore, the position obtained from that set of stretches can correspond to any position of the airplane movement during Δt s. Then, the inherent inaccuracy of the method may be up to $v_{max} \cdot \Delta t = 4.95$ m where v_{max} is the maximum speed of the airplane (see section below).

Calculation of relative Doppler stretch

In the experimental test, the ambiguity function has been computed for all possible values of Doppler stretch satisfying eq.(3.24). The Doppler stretch resolution $\Delta\delta f$ has been the same as used on computer simulations, 10^{-4}. The value of $k\Delta\delta f$ ($k \in \mathbb{N}$) reaching the maximum of the ambiguity function corresponds to the searched Doppler stretch δf_{mn}. All 42 values of Doppler stretch have been used to locate the radio control airplane.

Calculation of aircraft position

A maximum speed for each spatial coordinate may be chosen in order to define the solution search space $I \subseteq \mathbb{R}^6$ of the genetic algorithm (see section 3.2.3). As mentioned in section 5.1.2, the radio control airplane used for this test can reach a maximum speed of 33 m/s. Therefore, the search space for the speed in the x (Easting) direction and in the y (Northing) direction has been set to $[0; 33]$ m/s and in the z direction to $[0; 10]$ m/s.

5.2 Experimental test analysis

This section discusses different limitations of the experimental validation carried out. The inevitable oscillatory trajectory of the airplane and the inaccuracy of both the GPS mounted on the airplane and the GPS positioning the microphones are sources of error for the acoustic method inherent to the experimental test. These limitations are assessed in this section prior to the discussion of the acoustic method results.

5.2.1 Influence of the airplane positioning

Taking into account the challenge of the present experimental test discussed at the beginning of chapter 5, the pilot of the radio control airplane has been told to overfly the airfield at an altitude and speed as constants as possible. The microphones has been distributed as described in section 5.1.4 assuming an overflight of the airplane at constant altitude of 33 m and constant speed of 26 m/s (see fig.5.6). Moreover, keeping a constant speed will cause the airplane noise frequency spectrum to be stationary. The airplane trajectory given by the GPS mounted on it, what will be further called in the text real airplane position, is depicted (in gray) in fig.5.7 together with the expected trajectory (in black) used to distribute the microphones.

It can be seen that both paths seem to be similar but the oscillations of the real trajectory notably influence the relative Doppler stretches shown in fig.5.8a. Figure 5.8b represents the time evolution of the 42 relative Doppler stretches assuming the airplane travels along the expected trajectory at constant altitude and constant speed. Note that if the speed of the airplane remains constant, relative Doppler stretches are not influenced by the airplane speed since expression (3.18) can be rewritten as

$$\delta f_{mn} = \frac{\frac{c}{|\boldsymbol{v}|} - \cos(\alpha_n)}{\frac{c}{|\boldsymbol{v}|} - \cos(\alpha_m)}. \tag{5.1}$$

The term $\frac{c}{|\boldsymbol{v}|}$ does not vary along the airplane trajectory and thus, the angles α_n and α_m are the only responsible of the Doppler stretch variations. Figures 5.9a and 5.9b represent the evolution of the angles α_n between the airplane velocity $\boldsymbol{v}$ and the pathlength vector $\boldsymbol{q}_n$ pointing from the airplane to the receiver n (see fig.4.4) for the real and expected airplane trajectory respectively.

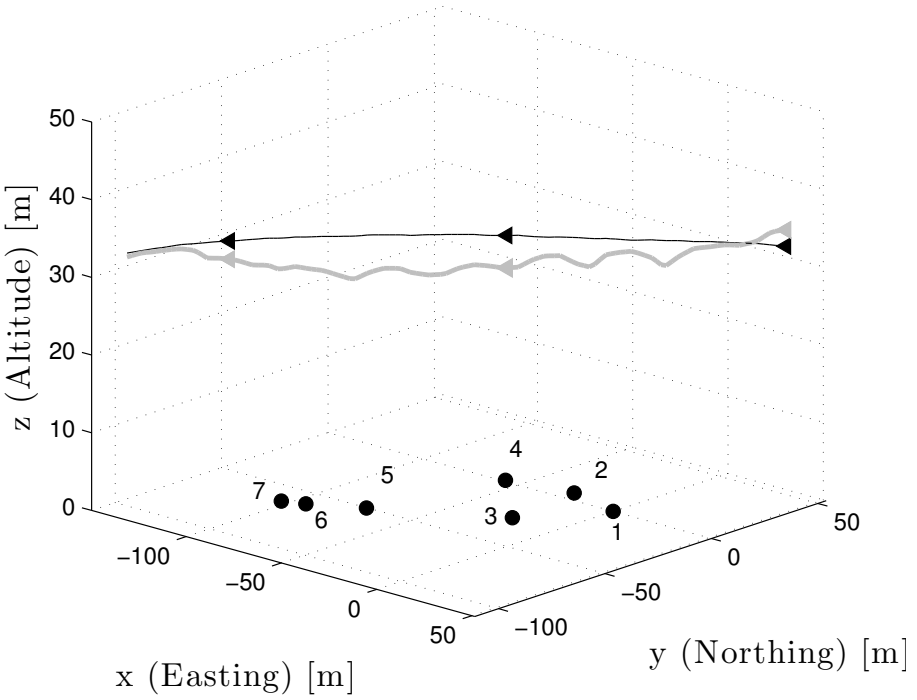

FIGURE 5.7: Expected (in black) and real (in gray) trajectories of the radio control together with the distributed microphones

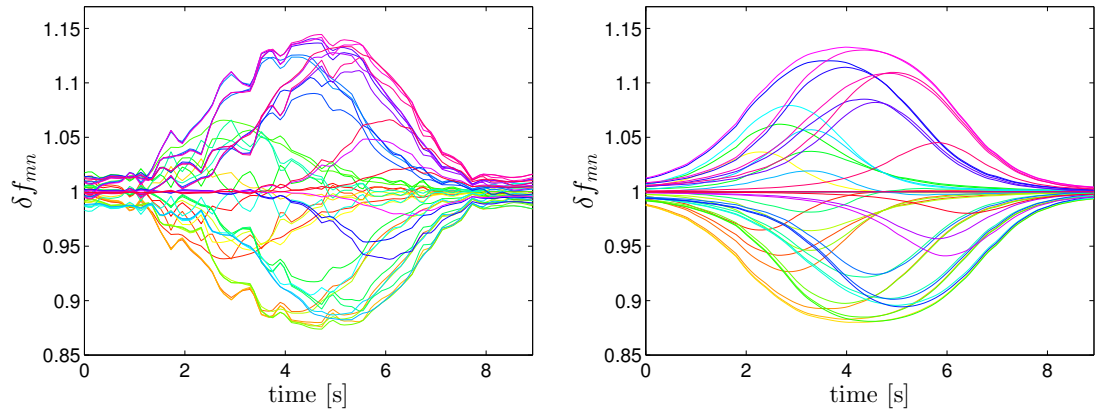

a) Time evolution of the 42 relative Doppler stretches computed from the real trajectory of the airplane

b) Time evolution of the 42 relative Doppler stretches computed assuming the expected trajectory of the airplane with constant altitude and constant speed

FIGURE 5.8

Significant variations of the relative Doppler stretches δf_{mn} in short time intervals can be observed in fig.5.8a due to the variations of α_n and α_m seen in fig.5.9a arising from the oscillations of the airplane real trajectory (fig.5.7). This fact will difficult the acoustic

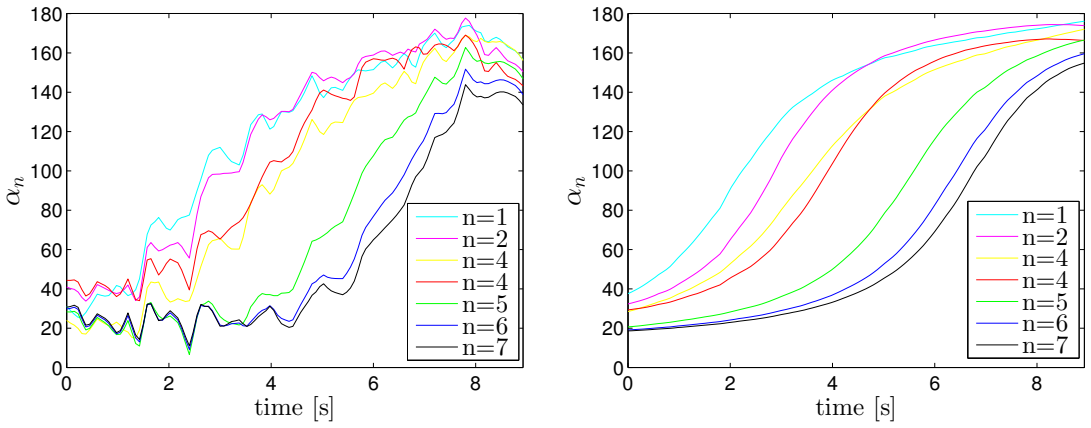

a) Time evolution of the angle α_n between the airplane velocity $\boldsymbol{v}$ and the pathlength vector $\boldsymbol{q}_n$ pointing from the airplane to the receiver n for the real airplane trajectory

b) Time evolution of the angle α_n between the airplane velocity $\boldsymbol{v}$ and the pathlength vector $\boldsymbol{q}_n$ pointing from the airplane to the receiver n for the expected airplane trajectory

FIGURE 5.9

method to estimate Doppler stretches and thus, to estimate accurate airplane positions. Moreover, the frequency spectrum emitted by the airplane will not remain stationary along the path due to real velocity evolution showed in fig.5.10, which depicts the constant expected velocity of modulus 26 m/s (in black) and the real velocity given by the GPS (in gray).

Therefore, the challenge for the experimental validation of the acoustic method has been proven prior to results.

Note furthermore that the accuracy of the GPS and Multi2 used in the experimental test is 3 meters as mentioned in section 5.1.3. Therefore by definition, the real position of the airplane can be within a sphere of radius 3 meters centered around the provided position. Thus, note that what is called real position, is indeed, just an estimation of the real position with a 3 meters accuracy. This inaccuracy will affect the error estimation of the acoustic localization method, since this error is computed as the difference between the acoustically estimated and the real positions.

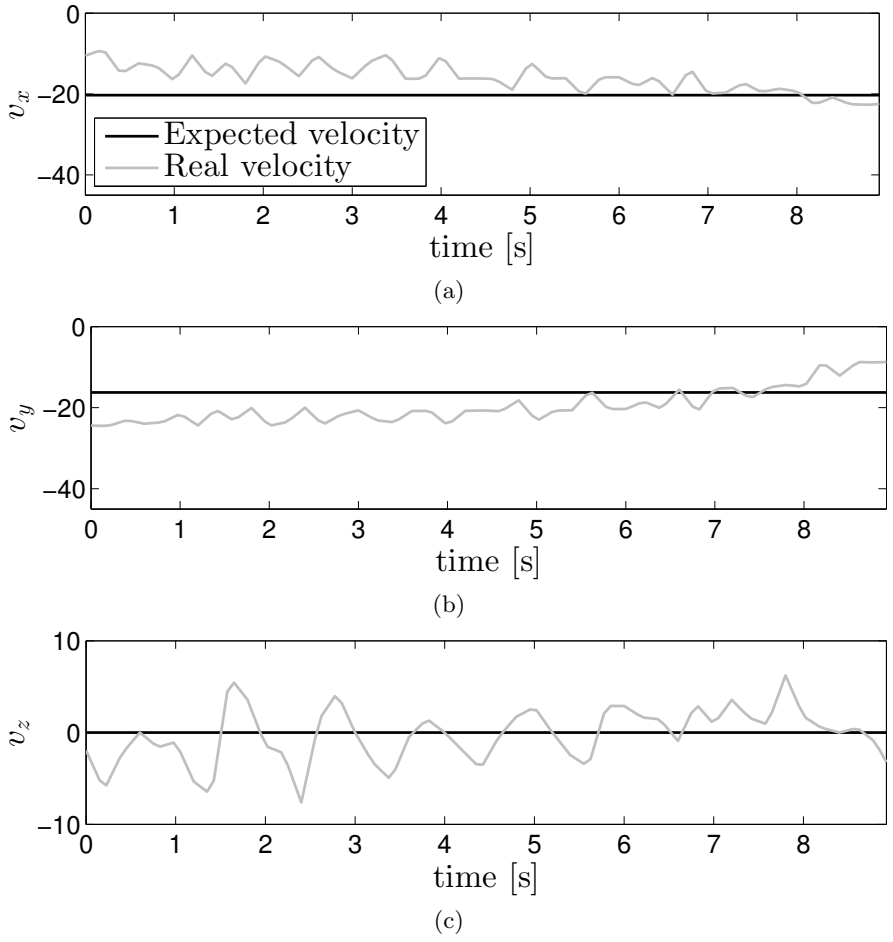

FIGURE 5.10: Expected and real velocities of the radio control airplane projected on: (a) the x-(Easting) direction, (b) the y-(Northing) direction, (c) the vertical direction z

5.2.2 Influence of the inaccuracy of the microphone positioning

As mentioned in section 5.1.3, the inaccuracy of the GPS used to obtain the microphone locations is up to 3 meters. To evaluate the influence of this uncertainty on the final position estimates, an error between 0 and 3 meters has been randomly added to all receiver coordinates in Table 5.2. The acoustic method has been tested using the theoretical (and not estimated by the acoustic method) relative Doppler stretches (fig.5.8a) computed from eq.(3.18) using the real airplane trajectory in fig. 5.7. In that way, the contribution of a possible inaccuracy on the Doppler stretches estimation is avoided. For statistical purposes, this test has been repeated 100 times and Table 5.4 shows the results averaged for all 100 tests.

TABLE 5.4: Maximum and mean localization errors obtained using the real flyover of the airplane (fig. 5.7) by randomly adding an error between 0 and 3 m to the microphone positions in Table 5.2.

u	$\max(Err_u)$ [m]	$\widehat{Err}_u$ [m]
x	19.9	8.1
y	18.2	7.2
z	12.7	4.6

Table 5.4 shows the averaged maximum localization error $\max(Err_u)$ and the mean localization error ($\widehat{Err}_u$) obtained for each coordinate $u = x, y, z$. It may be noticed that the absolute error for each coordinate is calculated by the absolute value of the difference between the location estimation given by the acoustic method and the real trajectory given by the GPS mounted on the airplane which already contains an uncertainty of 3 meters. The accuracy on the receivers positions is an important factor influencing the location results as shown in Table 5.4. Therefore, the errors of the experimental test can be expected to be of the same of magnitude than those presented in here since the receivers positions have an uncertainty due to the Garmin GPS inaccuracy. Note that due to the small distances between the microphones themselves as well as the microphones and the radio control airplane, the present experiment is a demanding test.

5.3 Results

5.3.1 Position estimation of a single flyover

The radio control airplane flies along the real trajectory in fig.5.7 during $t \in [0; 8]$ s and travels 210 meters. Figure 5.11 shows the time evolution of the absolute error $Err_u = |\widehat{p_u} - p_u|$ for each spatial coordinate $u = x, y, z$. Table 5.5 lists the maximum and mean errors, $\max(Err_u)$ and $\widehat{Err}_u$ (defined in section 4.4), for the time interval $t \in [0; 8]$ s. Three relevant sources of error are:

1. the uncertainty of the exact positions of the microphones due to the inaccuracy of the GPS
2. the uncertainty of the real position $p = (p_x, p_y, p_z)$ which has been considered error-free in this study
3. the inherent error of the method due to the non-stop airplane motion during the time interval Δt

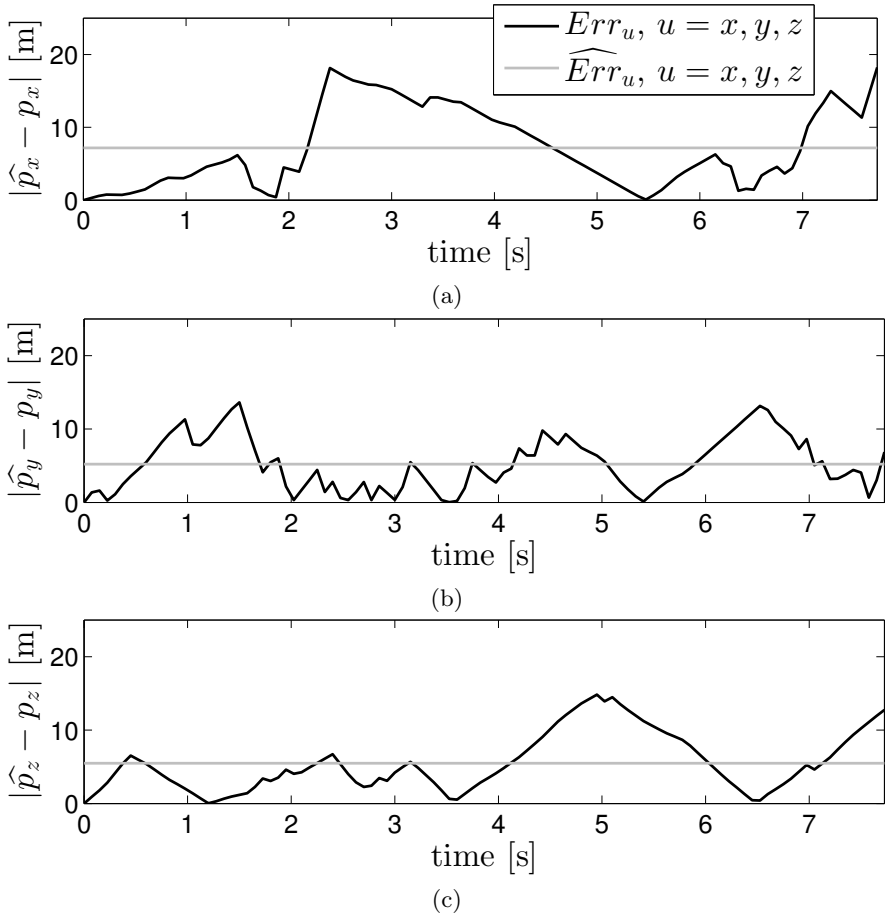

FIGURE 5.11: Time evolution of the absolute localization error along the flyover lasting 8 s for the three spatial coordinates: (a) x (Easting), (b) y (Northing) and (c) z (Altitude)

TABLE 5.5: Maximum and mean localization errors for each spatial coordinate x, y, z along the flyover lasting 8 s

u	$\max(Err_u)$ [m]	$\widehat{Err}_u$ [m]
x	18.2	7.17
y	13.63	5.21
z	14.82	5.48

The first and second sources of error have been discussed in section 5.2. The third source of error is discussed in here.

Each airplane position provided by the acoustic method is estimated by using signal portions of duration Δt and origin t^0. The estimated position is set to be $p(t^0+\Delta t/2)$, but indeed belongs to the spatial interval $[p(t^0); p(t^0+\Delta t)]$ due to the continuous motion of the airplane during Δt. The maximum possible difference between $p_u(t^0)$ and $p_u(t^0+\Delta t)$

for any spatial coordinate $u = x, y, z$ corresponds to $|v_{max}| \cdot \Delta t$. Thus, in this particular experimental test, the inherent error of the acoustic method due to the airplane motion during Δt is $|v_{max}| \cdot \Delta t = 4.95m$. Notice that the mean errors in Table 5.5 are of the same order of magnitude than this inevitable error.

Also as a consequence of the airplane motion during Δt s, the values of the estimated relative Doppler stretches $\widehat{\delta f_{mn}}$ are not constant from t^0 to $t^0 + \Delta t$. The maximum variation of these values for this experimental test during Δt s is 0.03 which is the inevitable uncertainty of all relative Doppler stretches. Figure 5.13 shows the absolute error committed on the computation of $\widehat{\delta f_{mn}}$ for $m \neq n$, $m, n \in \{1, ..7\}$, which is $|\widehat{\delta f}_{mn} - \delta f_{mn}|$. It can be seen that these errors are generally lower than 0.03. However, in particular time intervals 0.03 is exceeded. This phenomenon can be clearly observed in all plots of fig.5.13 for microphones $n = 5$ and $n = 6$ for which the Doppler stretch error $|\widehat{\delta f}_{mn} - \delta f_{mn}|$ exceeds 0.03 for $t \in [5; 6]$ s and $t \in [5.5; 6.5]$ s respectively. Section 4.1.2.1 discussed the relationship between an increase on the Doppler stretches error and the closest point of approach (CPA) of the source to the receivers observed from the computer simulation results. To corroborate it for the experimental test as well, fig.5.12 shows the distance evolution during $t \in [0; 8]$ between the radio control airplane and the microphones. It can be seen that the CPA for microphones $n = 5$ and $n = 6$ is reached during the time interval $[5; 6]$ s and $[5.5; 6.5]$ s respectively, which coincides with the already observed time intervals where their relative Doppler stretches error increases.

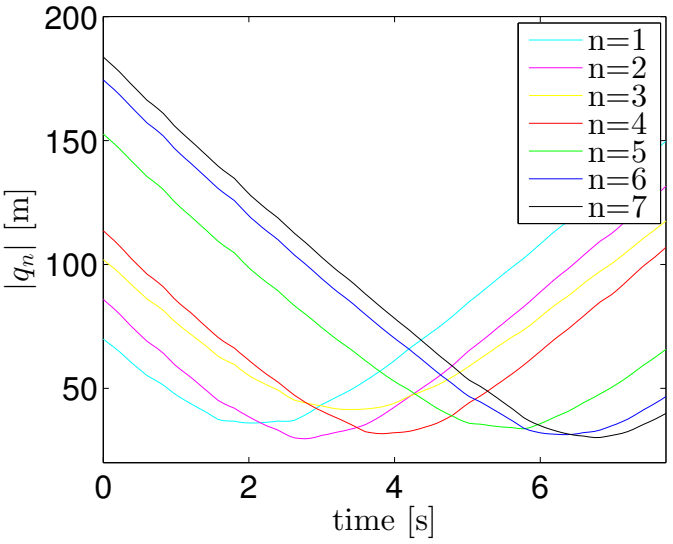

FIGURE 5.12: Distance between the aircraft and each receiver $n \in \{1, ..7\}$

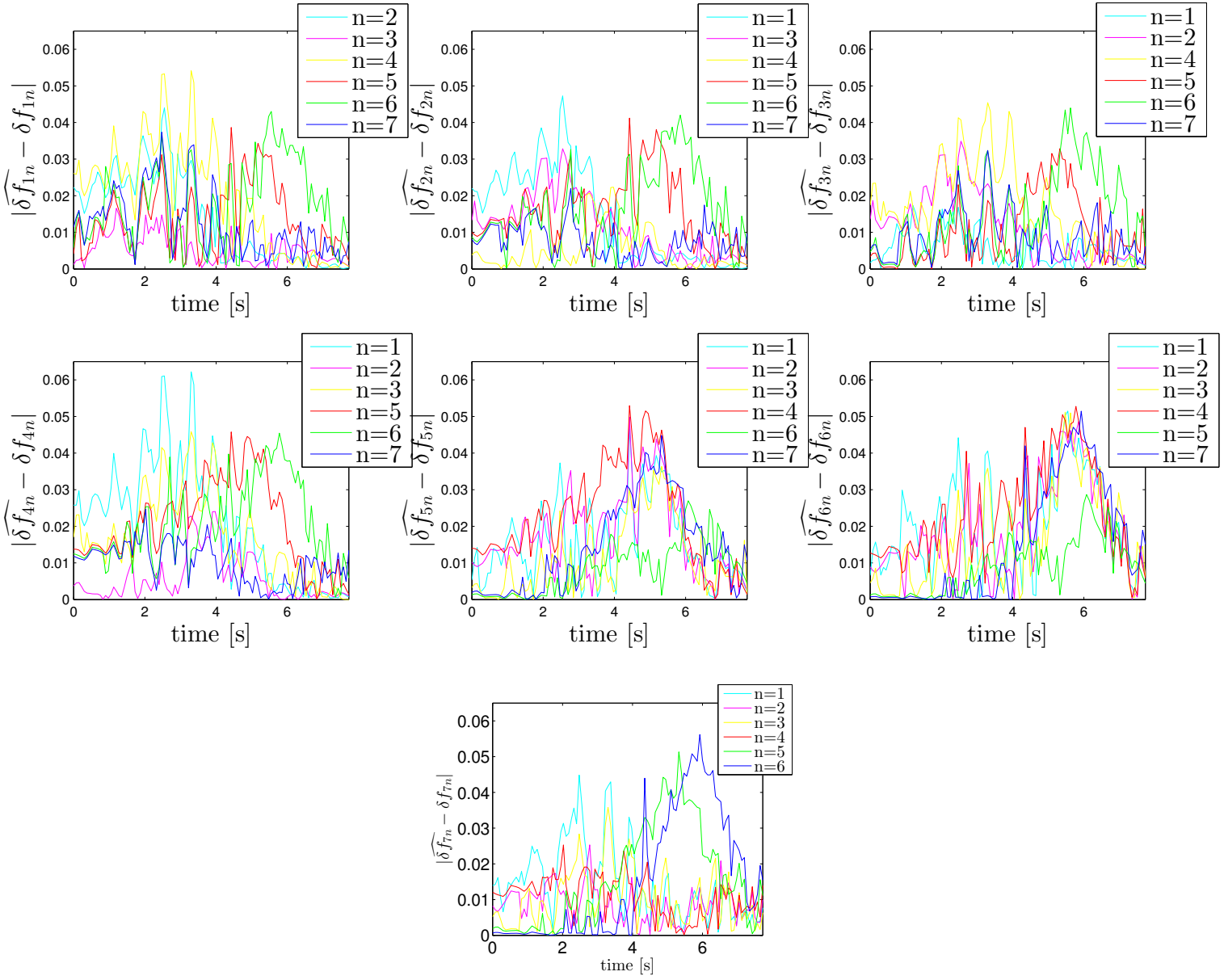

FIGURE 5.13: Time evolution of the Doppler stretches error δf_{mn} for $m \neq n$, $m, n \in \{1, ..7\}$

5.3.2 Position estimation of two consecutive flyovers

Figure 5.14 shows two consecutive real flyovers of the airplane, the first one corresponding to the real trajectory in fig.5.7. Figure 5.15 represents the real and acoustically estimated positions and fig.5.16 the real and estimates velocities during the 30 seconds of flight that the airplane lasts for. The continuous line in both figures corresponds to $p = (p_x, p_y, p_z)$ and $v = (v_x, v_y, v_z)$, the real position and velocity given by the GPS mounted on the airplane. The dashed line corresponds to $\widehat{p} = (\widehat{p_x}, \widehat{p_y}, \widehat{p_z})$ and $\widehat{v} = (\widehat{v_x}, \widehat{v_y}, \widehat{v_z})$, the estimated airplane states obtained from the acoustic method. For $t \in [0; 30]$ s, the radio control airplane has flied over the airfield in one direction, and after turning around sharply carries on a second fly-over in the opposite direction as can be seen in fig.5.14.

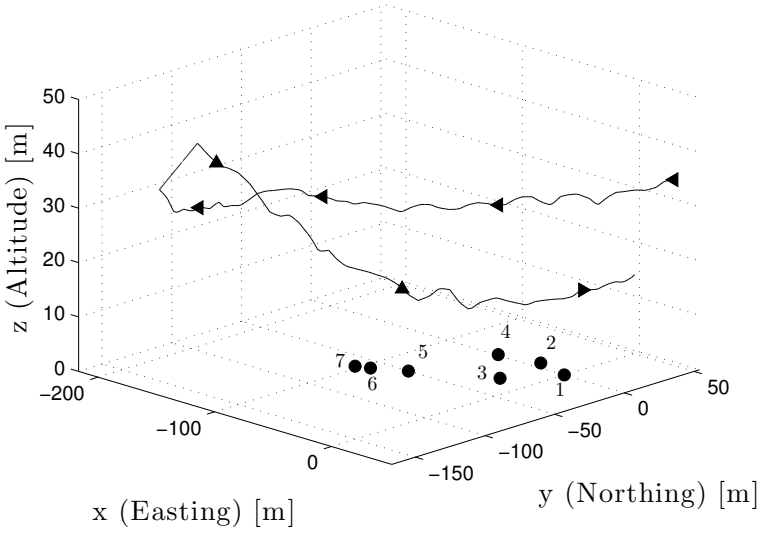

FIGURE 5.14: Microphone distribution together with two consecutive real flyover of the radio control airplane given by the GPS mounted on it

From time t=8 s to almost t=18 s both real and estimated locations shown in fig.5.15 differ notably. The reason of these differences lies on the values of the relative Doppler stretches δf_{mn} used to estimate the aircraft states. As mentioned in section 4.1.2.1 when all these values are similar to each other, the method fails to estimate the aircraft states. Figure 5.17 shows the time evolution of the 42 theoretical values of relative Doppler stretches during the 30 seconds of flight. It can be seen that from t=8s and t=18 s all relative Doppler stretches take almost the same value coinciding with the airplane flying away from the microphones. Thus, from the remarks of section 4.1.2.1, the position estimation given by the acoustic method fails as expected.

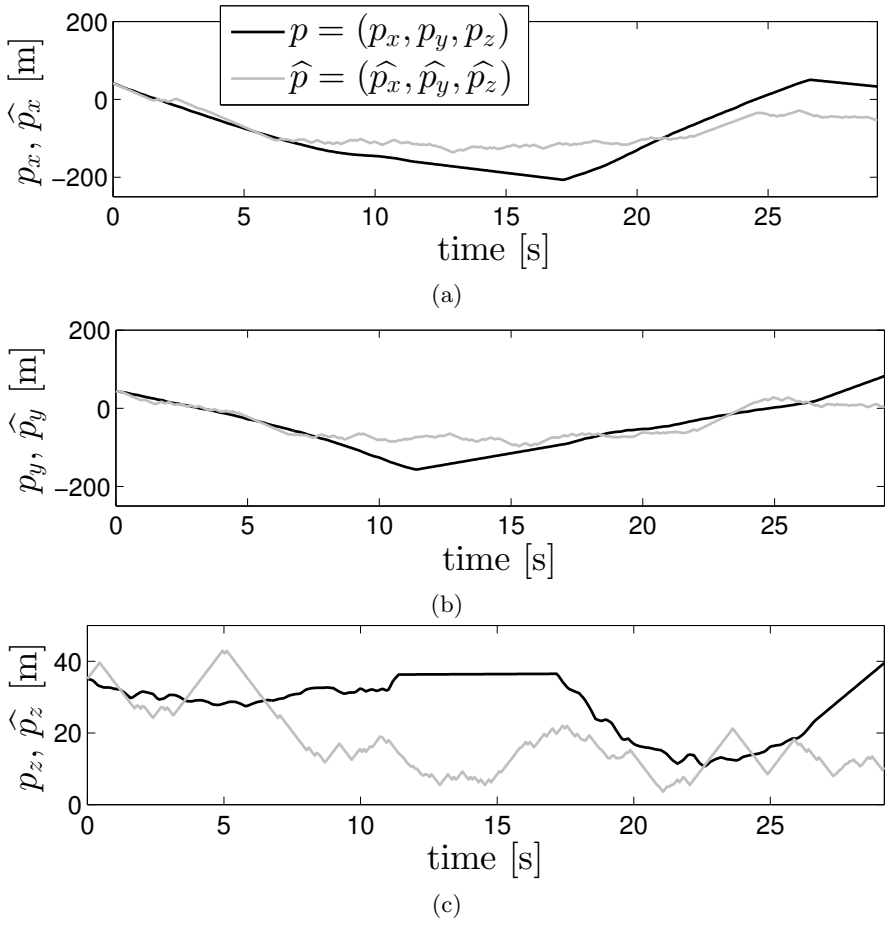

FIGURE 5.15: Radio control airplane localization given by the GPS ($p = (p_x, p_y, p_z)$) and estimated by the acoustic method ($\widehat{p} = (\widehat{p_x}, \widehat{p_y}, \widehat{p_z})$)

Despite of the localization failure between t=8 s and t=18 s (fig. 5.15), it can be observed that the estimated position of the airplane tends to the real trajectory from t=18 s onwards. The method seems to continue locating the airplane even if previously the localization has failed. Nevertheless, the error for $t \in [8; 18]$ s influences mainly the signals synchronization for $t > 18$ s (section 3.1.1) and thus, the accuracy of this second flyover is poor. Section 4.1.2.4 showed that the method is robust to initial position inaccuracies up to 170 m. Note that this value was obtained for the case of a commercial aircraft with long distances between source and receivers and a particular set of parameters. Therefore it is not applicable to the present experiment.

As mentioned in section 4.1.2.1, the use of more than seven microphones could avoid the problem of similarity between all relative Doppler stretches. Distributing other microphones farther away from the airfield would cover a longer part of the airplane flyover and would contribute to enlarge the localization given by the acoustic method.

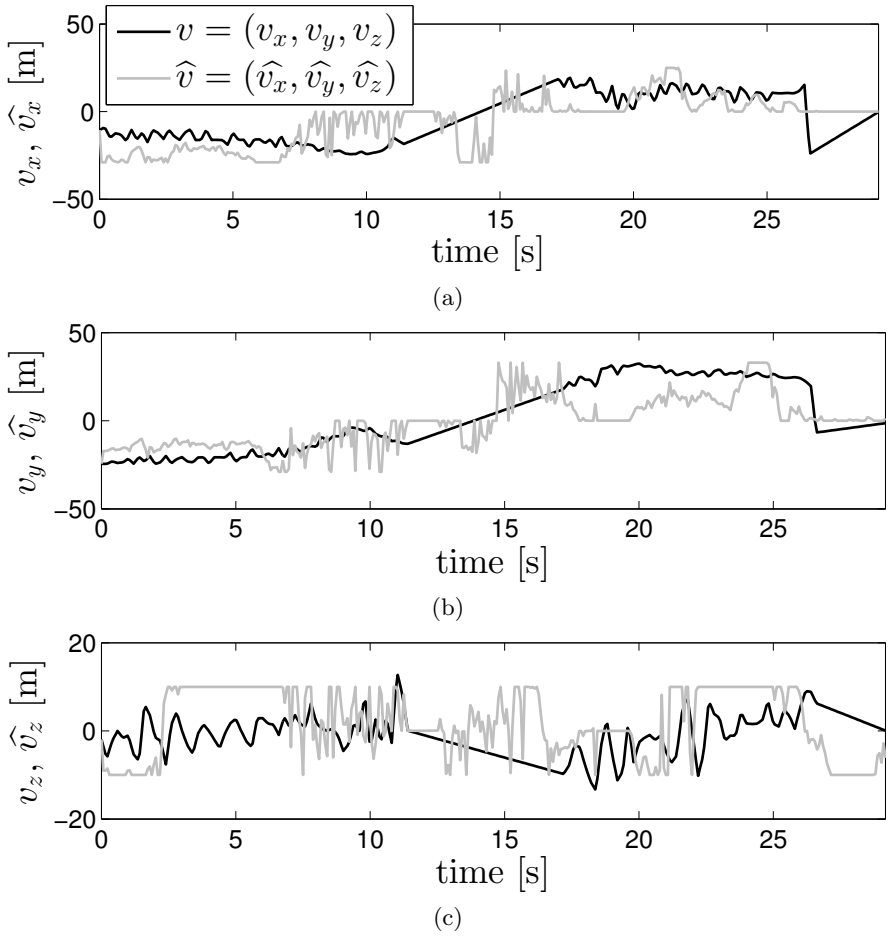

FIGURE 5.16: Velocity of the radio control airplane given by the GPS ($v = (v_x, v_y, v_z)$) and obtained from the acoustic method ($\widehat{v} = (\widehat{v_x}, \widehat{v_y}, \widehat{v_z})$)

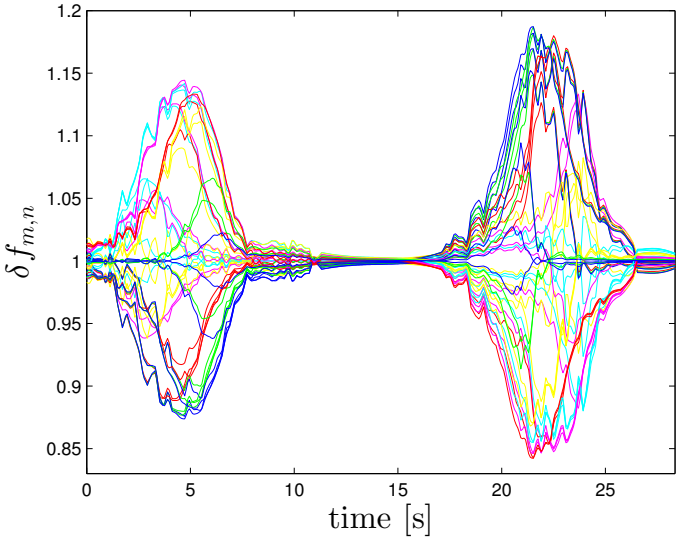

FIGURE 5.17: Time evolution of the 42 values of relative Doppler stretches δf_{mn} for $m \neq n$, $m, n \in \{1, ..7\}$ along two consecutive flyovers

Chapter 6

Conclusions

In this thesis a passive acoustic method to locate moving sound sources has been successfully applied to maneuvering aircraft. The method is based on the relation between the relative Doppler effect, observed in a set of at least seven receivers, and the position and velocity of the aircraft. The ambiguity function is used to calculate the relative Doppler stretch between the noise spectra received at each pair of microphones. The values obtained are introduced in the system of equations that relates the aircraft position and velocity to the relative Doppler stretches. A genetic algorithm is used to solve the system of equations to finally obtain the position and velocity of the source along the flight path.

Compared with existing passive acoustic methods aiming at locating aircraft, the method described in this thesis is suitable for all kind of aircraft, even if they are maneuvering, and is not restricted to aircraft flying at low heights above the ground. Moreover, it uses a mesh of single microphones instead of more complex arrangements such as microphone arrays or acoustic vector sensors. Notwithstanding, a limitation must be underlined here: the acoustic localization method assumes that microphones receive the direct noise from the aircraft emission. Receivers exposed to only diffracted or reflected noise may lead to miscalculation of the relative Doppler stretch, and thus the acoustic method may fail.

The effectiveness of the localization method has been firstly evaluated by computer simulation. Two different models have been considered for the propagation of the aircraft emitted noise.

With the aim of assessing the performance of the different steps of the acoustic method, a simple noise propagation model has been considered firstly. The model assumes the

sound propagation to be in a lossless medium. Thus, the geometrical spreading is the only effect to be taken into account on the sound propagation simulation. In this case, the aircraft has been simulated to fly along two different trajectories and three different microphone distributions have been tested. The results validate the good performance of the method considering that the location errors obtained from the simulations are of the same order of magnitude as the dimensions of a standard commercial aircraft regardless of the trajectory.

The acoustic method requires a previous knowledge of an initial position of the aircraft at a certain time instant. However, the initial position can be not as accurate as desired. The simulations show the robustness of the method in spite of the uncertainty in the aircraft initial position of as much as 170 m, and an uncertainty of the estimate of initial speed of as much as 33 m/s.

The performance of the ambiguity function in this application has been also tested by computer simulation showing that the contribution to the error in the localization of the aircraft is negligible.

The results for this first sound propagation model also show that the microphone distribution is an important factor that needs further study since the uncertainty in the calculated location of the aircraft increases whenever the aircraft is at the closest point of approach from any receiver (especially from the reference receiver), or when the relative Doppler stretches are nearly the same for several microphone pairs.

The second sound propagation model simulated in this thesis assumes an homogeneous but non lossless medium and considers the effect of the atmospheric absorption together with geometrical spreading. Geometrical spreading depends only on the distance from the receiver to the aircraft, and atmospheric attenuation of the emitted signal is moreover a function of the radiated frequency.

As a first step, the aircraft localization results for both simulated sound propagation models have been compared. The results obtained show that the introduction of atmospheric absorption increases the error of the aircraft localization with respect to the error obtained considering only geometrical spreading. However, this error is still acceptable and the influence of the atmospheric absorption does not alter the effectiveness of the aircraft location method.

The original description of the method suggests the use of a reference microphone to estimate the relative Doppler stretches from which the aircraft states are deduced. However, the choice of a microphone as a reference induces inaccuracy on both the Doppler stretches computation and aircraft position estimation. Two different alternatives to the use of a reference microphone have been proposed. One of them uses all possible values of Doppler stretches instead of the strictly six values obtained by using a reference microphone. The other one selects a set of six Doppler stretches as different as possible from all those estimated. Both alternatives show similar localization results and improve the original acoustic location method.

The aircraft localization method has also been tested for synchronization errors between the microphones. The errors considered are higher than the standard error ensured nowadays by providers of such sensors networks. The obtained results show the robustness of the method in front of inaccuracies in the microphones synchronization.

To validate the acoustic method, an experimental test has been carried out in an airfield using a radio control airplane and seven microphones distributed over the airfield area. From computer simulation results, it is seen that the microphones distribution affects the accuracy of the estimated airplane positions. The microphones need to be located so that the relative Doppler stretches influencing their frequency spectrum are as different as possible. This remark depends on the aircraft trajectory. Therefore, a flight path of constant altitude and constant speed has been considered to distribute the microphones prior to the experimental test.

The main purpose of the test was to compare the airplane trajectory estimated by the acoustic method and the trajectory given by a Global Positioning System mounted on the airplane. Nevertheless, the experimental validation has its own constraints due to the GPS devices used to locate both the radio control airplane and the set of seven microphones distributed over the airfield. The uncertainty of the microphone positioning may diminish the accuracy of the acoustic method down to a mean error around 8.1 m in the x-coordinate, 7.2 m in the y-coordinate and 4.6 m in the z-coordinate. Moreover, the GPS used to locate the airplane has an error up to 3 m meaning that indeed the given position is within a sphere of 3 m radius centered on it. Each coordinate of the position given by the GPS has then 3 m of uncertainty. The experimental results provide a mean error of 7.17 m in the x-coordinate, 5.21 m in the y-coordinate and 5.48 m in the z-coordinate in the airplane position. These errors do not exceed the expected errors due to the inaccuracy of the GPS devices used, meaning that the own error of the acoustic localization method is negligible compared to the constraints of the test.

Further developments

Results presented in this thesis show an encouraging scenario concerning further developments based on the acoustic localization method. Taking into account the general good performance of the method obtained from computer simulations and from the experimental test with a radio control airplane, the following extensions could be carried out.

- **Full scale validation of the acoustic localization method**

  As an immediate further work, a full scale validation of the method with a flight aircraft is currently been designed. To that aim, an autonomous telemetry system required to carry out the test is been built up and specially configured to acquire synchronously the acoustic data received by all microphones in use. At the moment, the system is not able to transmit data to a central terminal and thus, the signals are registered on a flash module connected to the acquisition module containing the microphone. The microphones have to be synchronized connected all together by cable to a central terminal (notebook or desktop PC) and distributed afterwards around the airport several kilometers far from each other. This distribution hinders the experimental test since at least seven people are required to locate the sensors as fast as possible and an accurate time control has to be managed from the synchronization process until all microphones are distributes.
  For this validation test, different aircraft takeoffs or landings should be selected prior to the experiment. This selection is important for several reasons: firstly, the acoustic method requires the prior knowledge of an aircraft position and the time when the aircraft was at this position; secondly, an appropriate distribution of the microphones can be easier chosen if at least the direction of the aircraft is previously known.

- **Study of the influence of aircrafts directivity**

  The directivity of a sound source is strongly dependent on the emitted frequency. As a consequence, the receivers distributed over an airport surroundings will receive the frequency spectrum emitted by the source modified differently. The directivity of jet commercial aircrafts influences the emitted noise more significantly than the directional radiation of light aircrafts or helicopters. It would be convenient to deeply study the directivity effect to assess and minimize its influence on the acoustic localization method.

- **Selection of optimum microphone locations**

  The microphones distribution is an influencing factor on the accuracy of the method. An appropriate location for the receivers requires the prior knowledge of the aircraft trajectory (which is unknown at the time of the microphones distribution) or at least its flight path direction. To improve the location accuracy of the acoustic method, further investigations could be carried out concerning an optimum microphones distribution.

- **Study of significant effects influencing the aircraft sound propagation**

  The wind, a non homogeneous propagation medium, or a non isospeed medium are different effects involved on the noise propagation from the sound source. Depending on the desired application of the acoustic localization method, it would be advantageous to previously model and simulate these effects and evaluate its influence on the acoustic localization method.

- **Completion of a noise monitoring system**

  As mentioned in the introduction of the present thesis, the development of the acoustic method arises from the desire to design, develop and implement an aircraft noise monitoring system independent from external data. To that aim, the acoustic localization method is only the first step. Further research could be done to obtain the sound power spectrum of the aircraft along its now known trajectory only from the acoustical data received by the microphones used for the acoustic localization method. Once the emitted sound power spectrum is known, the sound power signal could be backpropagated to estimate the real aircraft noise footprint over the vicinity of the airport.

- **Adaptive minimum noise route and aircraft operational configuration**

  In case the acoustic localization method could be executed on-line and the noise monitoring system could give the aircraft noise contribution at any spatial point almost instantaneously, an on-line optimization of the aircraft operational characteristics could be investigated in order to reduce the noise population exposure in the surroundings of a particular airport.

Bibliography

[1] *ISO 20906:2009 Acoustics - Acoustic Unattended monitoring of aircraft sound in the vicinity of airports*. ISO - International Organization for Standardization, 2009.

[2] On scheduling a multifunction radar. *Aerospace Science and Technology*, 11(4):289 – 294, 2007. ISSN 1270-9638. doi: 10.1016/j.ast.2007.01.006.

[3] Architecture of a multistatic fmcw direction-finding radar. *Aerospace Science and Technology*, 12(2):169 – 176, 2008. ISSN 1270-9638. doi: 10.1016/j.ast.2007.05.001.

[4] HW Chen and JW Zhao. On locating low altitude moving targets using a planar acoustic sensor array. *APPLIED ACOUSTICS*, 64(11):1087–1101, 2003.

[5] Huawei Chen and Junwei Zhao. On locating low altitude moving targets using a planar acoustic sensor array. *Applied Acoustics*, 64(11):1087 – 1101, Nov. 2003.

[6] K.W. Lo and B.G. Ferguson. Broadband passive acoustic technique for target motion parameter estimation. *IEEE Transactions on Aerospace and Electronic Systems*, 36(1):163 –175, Jan. 2000. ISSN 0018-9251. doi: 10.1109/7.826319.

[7] B. G. Fergusson. Time-delay estimation techniques applied to the acoustic detection of aircraft transits. *Journal of the Acoustical Society of America*, 106(1):255–264, 1999.

[8] Brian G. Ferguson. A ground-based narrow-band passive acoustic technique for estimating the altitude and speed of a propeller-driven aircraft. *The Journal of the Acoustical Society of America*, 92(3):1403–1407, 1992. doi: 10.1121/1.403934.

[9] Joseph C. Hassab, Brian W. Guimond, and Steven C. Nardone. Estimation of location and motion parameters of a moving source observed from a linear array. *The Journal of the Acoustical Society of America*, 70(4):1054–1061, 1981.

[10] Brian G. Ferguson. Variability in the passive ranging of acoustic sources in air using a wavefront curvature technique. *The Journal of the Acoustical Society of America*, 108(4):1535–1544, 2000.

[11] I. Hafizovic, C.C. Nilsen, and M. Kjolerbakken. Acoustic tracking of aircraft using a circular microphone array sensor. *IEEE International Symposium on Phased Array Systems and Technology*, pages 1025 –1032, Oct. 2010. doi: 10.1109/ARRAY.2010.5613233.

[12] F. Dommermuth and J. Schiller. Estimating the trajectory of an accelerationless aircraft by means of a stationary acoustic sensor. *The Journal of the Acoustical Society of America*, 76(4):1114–1122, 1984.

[13] F. M. Dommermuth. A simple procedure for tracking fast maneuvering aircraft using spatially distributed acoustic sensors. *The Journal of the Acoustical Society of America*, 82(4):1418–1424, 1987.

[14] Distributed mixed sensor aircraft tracking. *American Control Conference*.

[15] Shozo Mori, Kuo-Chu Chang, and Chee-Yee Chong. Tracking aircraft by acoustic sensors; multiple hypothesis approach applied to possibly unresolved measurements. *American Control Conference*, pages 1099 –1105, Jun. 1987.

[16] D.E. Dudgeon. Wideband array processing for acoustic detection and tracking of aircraft. *Nineteeth Asilomar Conference on Circuits, Systems and Computers*, pages 263 – 266, Nov. 1985.

[17] R Blumrich and J Altmann. Medium-range localisation of aircraft via triangulation. *Applied Acoustics*, 61(1):65 – 82, Sep. 2000.

[18] Brian G. Ferguson, Lionel G. Criswick, and Kam W. Lo. Locating far-field impulsive sound sources in air by triangulation. *The Journal of the Acoustical Society of America*, 111(1):104–116, 2002.

[19] M. Hawkes and A. Nehorai. Wideband source localization using a distributed acoustic vector-sensor array. *IEEE Transactions on Signal Processing*, 51(6):1479 – 1491, Jun. 2003.

[20] T. Basten, H. de Bree, and E. Tijs. Localization and tracking of aircraft with ground based 3d sounds probes. *3rd European Rotorcraft Forum*, 33(4):2282–2314, 2007.

[21] K.W. Lo, S.W. Perry, and B.G. Ferguson. Aircraft flight parameter estimation using acoustical lloyd's mirror effect. *IEEE Transactions on Aerospace and Electronic Systems*, 38(1):137 –151, Jan. 2002. ISSN 0018-9251. doi: 10.1109/7.993235.

[22] K.W. Lo, B.G. Ferguson, Yujin Gao, and A. Maguer. Aircraft flight parameter estimation using acoustic multipath delays. *IEEE Transactions on Aerospace and Electronic Systems*, 39(1):259 – 268, Jan. 2003. ISSN 0018-9251. doi: 10.1109/TAES.2003.1188908.

[23] Brian G. Ferguson and Barry Quinn. Application of the short-time fourier transform and the wigner-ville distribution to the acoustic localization of aircraft. *The Journal of the Acoustical Society of America*, 96(2):821–827, 1994.

[24] K.W. Lo and B.G. Ferguson. Flight path estimation using frequency measurements from a wide aperture acoustic array. *IEEE Transactions on Aerospace and Electronic Systems*, 37(2):685 –694, Apr. 2001.

[25] B.G. Ferguson and G.C. Speechley. Acoustic detection and localization of a turboprop aircraft by an array of hydrophones towed below the sea surface. *IEEE Journal of Oceanic Engineering*, 34(1):75 –82, Jan. 2009.

[26] H-E. de Bree, J. Wind, and S. Sadasivan. Broad banded acoustic vector sensors for outdoor monitoring propeller driven aircraft. *DAGA*, 2010.

[27] M. Genesca, J. Romeu, T. Pamies, and A. Balastegui. Passive acoustic method for tracking moving sound sources. *Acta Acustica united with Acustica*, 97(1):34–43, Jan. 2011.

[28] E. J. Kelly and R. P. Wishner. Matched-filter theory for high-velocity, accelerating targets. *IEEE Transactions on Military Electronics*, 9(1):56 –69, Jan. 1965. ISSN 0536-1559. doi: 10.1109/TME.1965.4323176.

[29] Qu Jin, Kon Max Wong, and Zhi-Quan Luo. The estimation of time delay and doppler stretch of wideband signals. *IEEE Transactions on Signal Processing*, 43 (4):904 –916, Apr. 1995. ISSN 1053-587X. doi: 10.1109/78.376843.

[30] L.G. Weiss. Wavelets and wideband correlation processing. *Signal Processing Magazine, IEEE*, 11(1):13 –32, jan. 1994. ISSN 1053-5888. doi: 10.1109/79.252866.

[31] X.X. Niu, P.C. Ching, and Y.T. Chan. Wavelet based approach for joint time delay and doppler stretch measurements. *IEEE Transactions on Aerospace and Electronic Systems*, 35(3):1111 –1119, Jul. 1999. ISSN 0018-9251. doi: 10.1109/7.784079.

[32] J. H. Holland. *Adaptation in Natural and Artificial Systems.* University of Michigan Press, 1975.

[33] A.P. Dowling and J.E.F. Williams. *Sound and sources of sound.* JOHN WILEY & SONS, INC., 605 Third Ave., New York, NY 10158, USA, 1983. ISBN 9780470273715.

[34] M. Genesca, J. Romeu, T. Pamies, and A. Sanchez. Real time aircraft fly-over noise discrimination. *Journal of Sound and Vibration*, 323, 2009.

[35] A.J. Chipperfield and P.J. Fleming. *"The MATLAB genetic algorithm toolbox".* IEE Colloquium on Applied Control Techniques Using MATLAB, Jan. 1995.

[36] *ISO 9613-1:1996 Attenuation of sound during propagation outdoors – Part 1: Calculation of the absorption of sound by the atmosphere.* ISO - International Organization for Standardization, 1996.

[37] *ISO 9613-2:1996 Attenuation of sound during propagation outdoors – Part 2: General method of calculation.* ISO - International Organization for Standardization, 1996.

[38] D.H.T. Bergmans and N.V. Bøgholm. Measuring environmental aircraft noise: combining new technologies with old ideas. *Inter-noise 2008 Shanghai - China*, 2008.

List of Figures

List of Tables